

SsODNet: Solar system Open Database Network[★]

J. Berthier¹, B. Carry², M. Mahlke², and J. Normand¹

¹ IMCCE, Observatoire de Paris, PSL Research University, CNRS, Sorbonne Universités, UPMC Univ Paris 06, Univ. Lille, France
e-mail: jerome.berthier@obspm.fr, jonathan.normand@obspm.fr

² Université Côte d’Azur, Observatoire de la Côte d’Azur, CNRS, Laboratoire Lagrange, France
e-mail: benoit.carry@oca.eu, max.mahlke@oca.eu

.../...

ABSTRACT

Context. The sample of Solar system objects has dramatically increased over the last decade. The number of measured properties (e.g., diameter, taxonomy, rotation period, thermal inertia, etc.) has expanded even more quickly. However, this wealth of information is spread over a myriad of studies, with different designations reported per object.

Aims. We provide a solution to the identification of Solar system objects based on any of their multiple names or designations. We also compile and rationalize their properties to provide an easy access to them. We aim to continuously update the database as new measurements become available.

Methods. We built a Web Service, SsODNet, which offers four access points, each corresponding to an identified necessity in the community: name resolution (quaero), compilation of a large corpus of properties (dataCloud), determination of the best estimate among compiled values (ssoCard), and a statistical description of the population (ssoBFT).

Results. The SsODNet interfaces are fully operational and freely accessible to everyone. The name resolver quaero translates any of the ~5.3 million designations of objects into their current and official designation. The dataCloud includes about 105 million parameters (osculating and proper elements, pair and family membership, diameter, albedo, mass, density, rotation period, spin coordinates, phase function parameters, colors, taxonomy, thermal inertia, and Yarkovsky drift) from over 3,000 articles (updated continuously). For each of the known asteroids and dwarf planets (~1.2 million), a ssoCard that provides a single best-estimate for each parameter is available. The SsODNet service provides these resources in a fraction of second upon query. Finally, the extensive ssoBFT table compiles all the best estimates in a single table for population-wide studies.

Key words. Astronomical data bases – Catalogs – Minor planets, asteroids: general

1. Introduction

The first decade of the 2000s saw an order of magnitude increase in the sample of known Solar System objects (SSOs) from roughly 50,000 to 600,000. While this number has doubled since, the revolution of most recent decade has seen an even faster growth on the part of the measured properties of these bodies. About 2000 diameters and albedo had been determined from IRAS mid-infrared observations (Tedesco et al., 2002) and over 150,000 are available today (e.g., Mainzer et al., 2011; Masiero et al., 2011; Grav et al., 2011). Hundreds of detections of the Yarkovsky effect (Vokrouhlický et al., 2015) are available (e.g., Del Vigna et al., 2019; Greenberg et al., 2020) just 20 years after the first-ever detection (Chesley et al., 2003).

This wealth of characterizations (e.g., colors, albedos, rotation periods, etc.) has allowed for multiple statistical studies on the forced orientation of family members by the Yarkovsky-O’Keefe-Radzievskii-Paddack (YORP) effect (Slivan, 2002; Hanuš et al., 2016), the compositional distribution of the asteroid belt (DeMeo & Carry, 2014), the size-frequency distribution of asteroid families (Parker et al., 2008; Masiero et al., 2013), the internal structure of minor bodies (Carry, 2012; Scheeres et al., 2015), and the origins of near-Earth asteroids (Perna et al., 2018; Devogèle et al., 2019; Binzel et al., 2019), among many others.

The benefit of all these developments has not, however, come to full fruition. If some catalogs are publicly available in machine-readable formats on the Planetary Data System¹ (PDS), the Centre de Données astronomiques de Strasbourg² (CDS), or alternative repositories (with unfortunately an endless variety of formats), a significant fraction of results have only been tabulated within the relevant papers. Some journals offer machine-readable versions of these tables on their online versions, but only for recent articles. Furthermore, the designation of small bodies often evolves over time, going from several possible provisional designations to a single number and then ultimately establishing an official name. Hence, the same object can be referred to with different labels in different studies, making its cross-identification over several sources a complex task. Accessing to all the characteristics of a given body or population can thus prove tedious and even impractical.

Compiling estimates of SSO properties and deriving the best estimate for each is of high practical relevance for the computation of ephemerides in the Virtual Observatory (VO) Web services we maintain (Miriade, SkyBoT, Berthier et al., 2006, 2008). Dynamical properties (i.e., osculating elements) are required to compute the position of SSOs and physical properties are required to predict their apparent aspect as seen by an observer, such as (i) the apparent magnitude in V band, rely-

[★] The ssoBFT catalog is available at the CDS via anonymous ftp to <http://cdsarc.u-strasbg.fr/> or via <http://cdsarc.u-strasbg.fr/viz-bin/qcat?J/A+A/xxx/Axxx>

¹ <https://pds.nasa.gov/>

² <https://cdsweb.u-strasbg.fr/>

ing on the phase function (HG or HG₁G₂, [Bowell et al., 1989](#); [Muinonen et al., 2010](#)), (ii) the apparent magnitude in any other band, requiring a color index derived from the spectral class (e.g., [DeMeo & Carry, 2013](#); [Popescu et al., 2018](#)), (iii) the flux at mid-infrared wavelengths, computed from the diameter and albedo through a thermal model ([Harris & Davies, 1999](#)), (iv) the shape and orientation of a target on the plane of the sky (often referred to as physical ephemerides), based on its 3D shape model, rotation period, and spin-vector coordinates (e.g., [Marciniak et al., 2012](#)).

Beyond the ephemerides computation, an extensive and rationalized compilation of SSO properties has many applications, from detailed in-depth studies on specific targets to population-wide statistical description of parameters. Over the years, publicly available compilations of data have flourished, for instance, the Jet Propulsion Laboratory Small Bodies Database³, the Las Cumbres Observatory NEOExchange⁴ ([Lister et al., 2021](#)), the Lowell observatory Minor Planet Services⁵ ([Moskovitz et al., 2021](#)), the NEOROCKS physical properties database⁶ ([Zinzi et al., 2021](#)), the Observatoire de la Côte d’Azur Minor Planet Physical Properties Catalog⁷ (MP3C, [Delbo et al., 2018](#)), the Size, Mass and Density of Asteroids (SiMDA⁸, [Kretlow, 2020](#)), and the SUPAERO ECOCEL⁹ ([Kovalenko et al., 2022](#)). While these services fulfill many of the community’s needs, most of them do not provide a fast machine-machine interface.

Thus, we have designed a fully scriptable Web Service named the Solar system Open Database Network (SsODNet) which is aimed at providing the best estimate of a variety of parameters for every SSO. Owing to the complexity of compiling SSO data as depicted hereinabove, SsODNet consists of a suite of chained steps: from the identification of objects to the massive compilation of data, ending with the selection of best estimates, and summarizing them in a table. As each of these steps represents a typical task relevant for the community, we propose a dedicated front-end (a Web service associated with an Application Programming Interface - API) for each.

In [Section 2](#), we describe how quaero builds a unique identifier for each object, associating all its aliases and providing the identity of the SSO. In [Section 3](#), we describe how dataCloud compiles the measurements and estimates of properties from many sources, providing the most-possible comprehensive data set of SSOs. In [Section 4](#), we describe how ssoCard provides the best estimate of each SSO property, and lists them in a single organized identify card. In [Section 5](#), we describe how ssoBFT summarizes the most-commonly requested of these parameters for all SSOs. We then describe how to query these services in [Section 6](#) before discussing the future developments of SsODNet in [Section 7](#).

2. Name resolver: quaero

The SsODNet.quaero name-resolution service is built to address the issue of identification of SSOs and, more generally, of all planetary and artificial objects gravitationally bound to a star. Upon the submission of any of the possible designations of a target, quaero returns its official or main designation, together with

all its aliases. To be compliant with the spirit of the VO (“name resolver”) quaero can also return the equatorial coordinates of the object at a given epoch.

2.1. Context

The Solar System is populated by widely different types of celestial bodies: from planets and their satellites to minor planets (comets, asteroids, Centaurs, Kuiper-belt objects, etc.) and their satellites, and further on to artificial satellites, space probes, and space debris. Since the first exoplanet detection by [Mayor & Queloz \(1995\)](#), today we know of about 5000 planetary objects that orbit around other stars than the Sun. A few rogue planets (e.g., OTS 44 or Cha 110913-773444) and two interstellar objects (1I/Oumuamua and 2I/Borisov) complete the picture of the planetary zoo.

The nomenclature of SSOs is entrusted to two groups under the auspices of the International Astronomical Union (IAU) Division F. The first is the Working Group for Planetary System Nomenclature (WG-PSN), which is in charge of naming features on planets, satellites, and asteroids. This group also names planets (although the IAU has not named a planet as of yet) and the natural satellites of major planets. The second is the Working Group for Small Bodies Nomenclature (WG-SBN), which is responsible for naming of all other small bodies (minor planets, satellites of minor planets, and comets). Both working groups share responsibility for naming dwarf planets ([IAU, 2020a](#)).

As of today, there are no official name for exoplanets assigned by the IAU. The public names, assigned through a public naming process such as NameExoWorlds¹⁰ is distinguished from the official scientific designation, which follows the rules of the system used for designating multiple-star systems as adopted by the IAU ([IAU, 2020b](#)).

Spacecraft, together with launchers, payloads, and space debris, are indexed for safety and cooperation purposes. They are usually named by their funders (space agencies, laboratories, or companies). They are also assigned an International Designator (COSPAR ID), under the responsibility of the *Committee on Space Research* (COSPAR) of the *International Council for Science* (ICSU), and a Satellite Catalog Number (NORAD ID) attributed by the *United States Space Command* (USSPACE-COM).

Since the designation of the major bodies of the Solar System (the Sun, the Moon, the eight planets), more than 1.2 million objects have been inventoried, classified, and named. As of today, there are more than 5.3 million designations used to name them all. Objects can have multiple designations owing to the evolution of knowledge as well as changes in nomenclature over time¹¹. We illustrate this with the first asteroid discovered in 1801: Ceres. It is classified today as a dwarf planet. Its official designation is “(1) Ceres:” a number in parenthesis followed by a name. This official designation thus already contains two labels. However, Ceres was also named using provisional designations over the years, assigned to past astrometric observations that had not been immediately connected to its orbit: “1801 AA,” “1899 OF,” and “1943 XB,” and the corresponding packed names¹² “I01A00A,” “I99O00F,” and “J43X00B”. Thus Ceres can be known by eight different names. The all-time

³ <https://ssd.jpl.nasa.gov/>

⁴ <https://neoexchange.lco.global/>

⁵ <https://asteroid.lowell.edu>

⁶ <https://neorocks.elecnor-deimos.com/web/guest/search-retrieval>

⁷ <https://mp3c.oca.eu>

⁸ <https://astro.kretlow.de/?SiMDA>

⁹ <http://www.ecocel-database.com>

¹⁰ <https://www.iau-100.org/name-exoworlds>

¹¹ <https://www.minorplanetcenter.net/iau/info/DesDoc.html>

¹² <https://www.minorplanetcenter.net/iau/info/PackedDes.html>

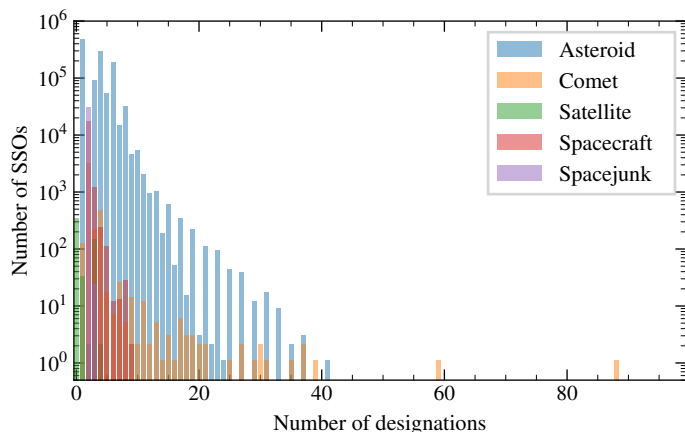


Fig. 1: Histogram of the number of designations for each class of object.

Table 1: Statistics of the number of SSO designations by object class.

Type	Number of designations			
	min	max	mean	σ
Asteroids	2	42	4	2
Comets	2	89	4	3
Dwarf planets	6	10	6	2
Planets	3	3	3	0
Satellites	2	6	2	1
Spacecrafts	3	10	3	1
Spacejunks	3	4	3	0
Exoplanets	1	2	1	0

record is held by comets P/Halley (1P), with 59 designations, and P/Encke (2P), with 89 designations. We present in Figure 1 the distribution of the number of designations by type of SSOs and we present a summary in Table 1.

2.2. Quaero: /k^wæ.ɾoː/

This is the core of SsODNet. It ensures the reliability of the naming of SSOs and it allows us to cross-match identifications between their actual names and the designations used over time in the various data sets. In August 2022, we counted 1 288 838 solar and extra-solar objects for 5 360 208 designations (1:4 ratio).

Overall, SsODNet.quaero is designed to fulfill four main functionalities: 1) to identify a SSO from its designation; 2) to explore the naming of SSOs using wildcard, regular expression, or fuzziness; 3) to resolve the name of a SSO into sky coordinates; and 4) to provide an autocomplete feature that can be used to offer SSO name suggestions when a user types in an input field.

To achieve this goal, once a week we gather all the available planetary object designations from the Minor Planet Center (Marsden, 1980) for asteroids and dwarf planets, the IMCCE’s CometPro Database (Rocher & Cavelier, 1996) for comets, the Extrasolar Planets Encyclopaedia (Exoplanet-Team, 2021) for exoplanets, and CelesTrak (Kelso, 2021) for spacecrafts and debris. These designations are then stored and indexed in a dedicated database.

We use the NoSQL database Elasticsearch¹³ to manage the millions of designations. It is a full-text search engine based on

¹³ <https://www.elastic.co/>

the Apache Lucene library¹⁴. Each object is defined by a set of fields (document) defining its Id, name, aliases, parent, type, and so on. Documents are stored in an Elasticsearch index as JSON-format data. By default, Elasticsearch tries to guess the correct mapping for fields, but to meet the challenges of planetary object identification, we specified our own mapping.

If SSO designations are indexed as individual strings, then a user can only find whole names. To allow for the search of a name on a part of a designation, we decompose all the SSO designations into small chunks (tokens). However, at this step, each token is still matched literally. This means (among other things) that a search for a name with or without an accent or a special character, or one with mixed lowercase and uppercase characters, would possibly not result in a match with any name. To solve this issue, we defined the normalization rules to allow for the matching of tokens that are not exactly the same as the search names, but similar enough to still be relevant. For the full technical information, we refer to the documentation¹⁵ of the SsODNet.quaero API.

3. Compilation of properties: dataCloud

The SsODNet.dataCloud service is designed to compile all published measurements and estimates of SSO properties. The dataCloud uses SsODNet.quaero to identify objects over their multiple designations. It also associates every estimate with a bibliographic reference and a method. Upon request, the dataCloud returns all the estimates of a given property or parameter for the requested SSO.

3.1. Context

Starting with the planetary motion (Newton, 1760), the first studies of SSOs focused on their dynamics (Gauss, 1809), which is required to compute their ephemerides. From the distribution of their orbital elements, Hirayama (1918) discovered the dynamical families. Time-series photometry has led to the determination of numerous rotation periods in the first half of the twentieth century (e.g., Bailey & Pickering, 1913). The 1970s saw the advent of compositional and physical studies, with the first studies of diameter and albedo (e.g., Cruikshank & Morrison, 1973), mass and, hence, the density (Schubart, 1974), along with the spectrophotometry and taxonomy (e.g., Chapman et al., 1975). The handful of SSOs with spin-vector coordinates and triaxial dimensions of the 1980s (Drummond & Cocke, 1989) grew to several hundreds in the 2000s thanks to the light-curve inversion technique (Kaasalainen & Torppa, 2001). Similarly, estimates of thermal inertia and Yarkovsky drift are common nowadays (Hanuš et al., 2018; Greenberg et al., 2020), even though the first studies were completed only two decades ago (Lagerros, 1996; Chesley et al., 2003).

Benefiting from these progresses is complex, however, as the fast-growing number of measured properties is spread over a myriad of articles. Machine-readable catalogs delivered by authors to the PDS or the CDS only represent the tip of the iceberg. Furthermore, there is a large heterogeneity in how SSOs are labeled (number, name, packed designation, etc.) and in how quantities are reported: masses, M , in terms of kg or solar masses (M_{\odot}) or as a GM product or the albedo in linear or logarithmic scale, for instance.

¹⁴ <https://lucene.apache.org/>

¹⁵ <https://doc.ssodnet.imcce.fr/quaero.html>

The sample size of individual articles may be small, but their sum is large. In particular, some size-limited sample may be extremely valuable, such as results on a single target obtained during a spacecraft rendezvous for example. Therefore, the goal of compiling every estimate should not be overlooked by the community.

SsODNet.dataCloud compiles in a single database as many estimates as possible for a variety of SSO properties. Such a centralization of data may appear anachronistic in the current landscape of connections to remote databases, such as what is regularly done in the VO (Bayo et al., 2008). It is, however, required here. First, the remote databases do not exist. Second, owing to the issue of SSO naming, on-the-fly cross-matches between resources would be slow upon query. We chose to place the workload on the server side, in an asynchronous process, to provide a fast service to users. Such a solution is already used for the ESA Gaia archive¹⁶, in which time-consuming cross-matches of Gaia catalog (Gaia Collaboration et al., 2016, 2018, 2021) with other common large catalogs (e.g., SDSS DR9, 2MASS, allWISE, Ahn et al., 2012; Skrutskie et al., 2006; Wright et al., 2010; Cutri et al., 2013) are already computed and stored (see details in Marrese et al., 2017).

3.2. Method

The design of the dataCloud is very simple: the parameters are grouped by collection of properties in SQL tables, such as diameter and albedo (as they are seldom derived independently), mass, thermal inertia, taxonomy, astrometry (the MPCAT-OBS database, MPC, 2021), and so on. There are a few exceptions to this general scheme. The osculating elements of asteroids from the Minor Planet Center (MPC, Marsden, 1980) and the Lowell observatory (Bowell et al., 1994), as well as those of comets from the IMCCE (Rocher & Cavelier, 1996), are stored in separated tables. The Appendix A provides the list of collections composing the dataCloud ecosystem.

Each entry of tables corresponds to a single determination of a parameter for a given target. Parameters are stored with their uncertainties, the method used to obtain them (see Appendix B), a selection flag (used to discriminate among estimates; see Section 4), and the bibliographic reference of the source of data. A given SSO, or bibliographic reference, may be repeated multiple times: some studies include many objects and the same SSO may have been analyzed in multiple studies. Figure 2 shows the distribution over time of the publications (currently 3007) used to build the dataCloud database. For convenience, a file compiling all the bibliographic references in bibtex format is available¹⁷.

A key aspect of the collections is the unique identifier assigned to each SSO, built upon their name and used to identify them across tables. At every update of the database, the name of each SSO (as published by authors) is tested with SsODNet.quaero and updated upon ingestion. Hence, all properties are linked together using the most up-to-date designation.

For each parameter, we started the compilation from scratch, individually adding each bibliographic reference. The only exceptions to this are the masses and the spins. For both, we first input a previous compilation of data, taken from Carry (2012) and Warner et al. (2021) respectively.

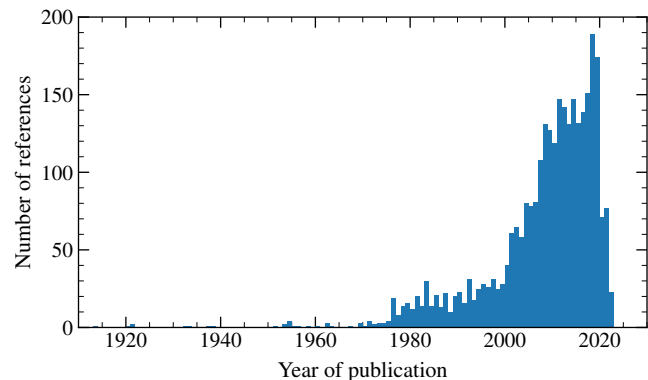


Fig. 2: Years of publication of bibliographic references used to populate SsODNet.dataCloud.

4. Selection of the best estimates: ssoCard

The SsODNet.ssoCard provides a practical solution to the question of finding the best estimate for a wide range of parameters of SSOs. From the dataCloud, it builds the resume of each SSO, named ssoCard. These ssoCard are small files that can be easily downloaded and read upon user request. The present first release of SsODNet.ssoCard proposes ssoCard for asteroids and dwarf planets only. We plan to offer ssoCard for other types of SSOs (comets, satellites) in subsequent releases (see Section 7).

4.1. Context

Among the hundreds of articles compiled in the dataCloud, a significant fraction report the same parameter for a given SSO. A question then arises about the most optimal way to choose a value. A simple statistical averaging cannot address the question: some methods are intrinsically more precise than others and some are direct measurements, while others are model-dependent. Moreover, uncertainties associated with values often do not account for possible biases, namely, for external errors. This implies that the choice of the best value cannot entirely rely on criteria that are based on the repeatability of the measurements.

The structure and format of data must also be addressed. The usual table format (i.e., rows and columns) is not very well adapted to these purposes. Some SSOs have estimates across a wide variety of parameters (osculating elements, proper elements, diameter, mass, density, colors across many filters, taxonomy, and so forth), while others have a few parameters only (e.g., osculating elements). Structuring the data in a flat 2D table implies that a vast majority of cells will be empty. With the current data in SsODNet, the filling factor of such a table would only be ~15% (see Section 5).

Furthermore, the association of data with meta-data (i.e., method, bibliographic reference, and units) is also an issue with regard to the table format. Considering that a human-readable bibliographic reference is composed of at least four fields (title, authors, year, bibcode), the number of columns will increase by a factor of four for each group of properties. In the current ecosystem of SsODNet.dataCloud, composed of 15 collections exposing 591 fields, it would imply a final table composed of 651 columns.

Considering all these elements, we chose to structure the parameters in a key-value data format allowing for nested objects

¹⁶ <https://gea.esac.esa.int/archive/>

¹⁷ <https://ssp.imcce.fr/data/ssodnet.bib>

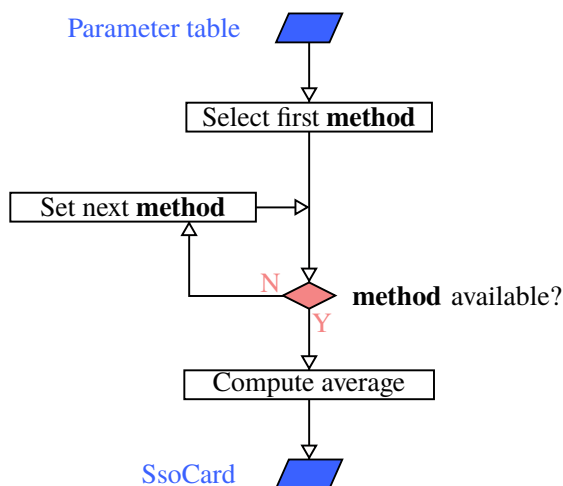


Fig. 3: General workflow used to compute the best estimate of each parameter.

and arrays. We chose the open standard file format JSON (Bray, 2017). A XML-based format such as VOTable¹⁸ could have been suitable to include metadata, but given it is rather verbose in nature, it would significantly increase the volume of data to exchange.

4.2. Method

The best estimate for each SSO property depends mainly on the method used to measure it: for example, a direct measurement from an in situ space mission can be considered to be more valuable than an indirect determination based on telescopic observations acquired from the Earth. Similarly, a modern measurement is often more accurate than an earlier measurement owing to technological advances. On the other hand, an old value remains useful because it increases the temporal validity of the measurement and can be unique. Finally, the accuracy (closeness to the true value) and precision (repeatability of the value) of measurements must be considered to choose a particular value among a data set or to compute a statistical average.

For each set of properties, we defined a decision tree that is schematized in Figure 3. The methods are ordered in a preferential order. Among the ordered methods, the first available is chosen, and the weighted average μ is computed from N multiple estimates, x_i , by the least-squares estimator:

$$\mu = \frac{\sum_{i=1}^N w_i x_i}{\sum_{i=1}^N w_i}, \quad (1)$$

where $w_i = 1/\sigma_i^2$ and $\sigma_i = (\sigma_{+,i} - \sigma_{-,i})/2$ is the arithmetic mean of the upper and lower uncertainties $\sigma_{+,i}$ and $\sigma_{-,i}$.

Similarly, the upper and lower uncertainties on μ are computed as:

$$\sigma_{\pm} = \frac{\sum_{i=1}^N w_i \sigma_{\pm,i}}{\sum_{i=1}^N w_i}, \quad \text{with } w_i = 1/\sigma_{\pm,i}^2. \quad (2)$$

When the uncertainty of a value is unknown, we set it to 100% of the value to weight the mean. At this stage, the

¹⁸ <https://ivoa.net/documents/VOTable/>

N estimates used to compute the average may be less than the total number of estimates available. Every single entry in SsODNet.dataCloud has a selection flag (see Section 3). Only three values are possible for this flag: -1, 0 (default), and 1. Any estimate with a selection flag of -1 is discarded from the computation of the best estimate. If an estimate is flagged with 1, it is considered to be the best estimate (we refrain from using it). The overwhelming majority of entries in dataCloud have a selection flag of 0.

We describe below how the preferential order is defined for each parameter and we provide the exhaustive order in Appendix C. Exceptions to this scheme of averaging include family membership, albedo, taxonomy, and the orbital elements of SSOs.

4.2.1. Osculating elements

We store in SsODNet.dataCloud the complete catalogs of osculating elements of asteroids and dwarf planets proposed by the MPC (mpcorb, Marsden, 1980) and the Lowell Observatory (astorb, Bowell et al., 1994). Osculating elements are a consistent ensemble for each SSO. Thus, we do not select them individually, but as a group. As the primary source, we chose the astorb catalog for the ssoCard, completed with elements from mpcorb for SSOs that are not listed in astorb.

For each SSO, we used its osculating elements (semi-major axis, a , inclination, i , and eccentricity, e) to compute its Tisserand parameter (Tisserand, 1889) with Jupiter (T_J) and report it in the ssoCard:

$$T_J = \frac{a_J}{a} + 2 \cos i \sqrt{\frac{a}{a_J} (1 - e^2)}, \quad (3)$$

taking $a_J = 5.203\,363\,01$ au (mean J2000 orbital element).

4.2.2. Proper elements

Until recently, the only source of proper elements was the Asteroid-Dynamical Site¹⁹ (AstDyS, Knežević & Milani, 2003, 2012). The computations used either the analytical or numerical methods by Milani & Knežević (1990, 1994), Knežević & Milani (2000), and Knežević et al. (2002). More recently, Vinogradova (2019) introduced the empirical approach.

The most recent and largest update on asteroid proper elements is provided by the Asteroid Families Portal²⁰ (Novakovic & Radovic, 2019). It thus prevails over the others and we included it in SsODNet.dataCloud to report proper elements of SSOs in ssoCard. As Jupiter Trojans and KBOs are not reported in this catalog, we complemented it with the proper elements for these populations from AstDyS.

4.2.3. Families

The existence of asteroid families has been recognized over a century ago (Hirayama, 1918). Many authors have been working on the subject over the last decades, using mainly the Hierarchical Clustering Method (HCM, Zappala et al., 1990). A new method has recently emerged, called V-shape (Bolin et al., 2017).

As families are groups of SSOs, the selection is family-based in contrast with other parameters that are SSO-based. We

¹⁹ <https://newton.spacedys.com/astdys/>

²⁰ <http://asteroids.matf.bg.ac.rs/fam/>

set as a reference the most-recent large-scale study (presently, [Vinogradova, 2019](#)). All the families listed in the reference are considered valid and SSOs belonging to these families have a family item in their ssoCard describing their membership.

We then complete these families with those reported in the other studies listed in SsODNet.dataCloud. We distinguish two cases. For articles studying families in general (e.g., [Milani et al., 2014](#)), we add the families not reported in the reference data set. A complexity arises from the fact that different authors may label the same family under different names (such as Minerva and Gefion being two names pointing at the same family, [Milani et al., 2014](#); [Nesvorný, 2015](#)). We thus compute the fraction of common members between reported families. Whenever the overlap is smaller than 10%, the families are considered different. Alternatively, if one family is significantly smaller than the other (at most 20% in number of members), we include it to the list of families as it is likely a sub-family of the larger one.

For articles focusing on a single family (e.g., [Tsirvoulis, 2019](#)), we consider that they supersede the reference data set. If the family they describe is present in the reference data set, we replace the family membership of all SSOs in the family. If not, we simply add the new family (e.g., [Delbo et al., 2019](#)). We illustrate the dynamical families of in the asteroid belt available in SsODNet in [Figure 4](#).

4.2.4. Pairs

Pairs of asteroids are objects on highly similar heliocentric orbits, first discovered by [Vokrouhlický & Nesvorný \(2008\)](#). They are similar to dynamical families with only two members and are thought to be formed by rotational fission ([Scheeres, 2007](#); [Pravec et al., 2010](#)). They are identified from the distance d between their orbits (in $\text{m}\cdot\text{s}^{-1}$):

$$\left(\frac{d}{na}\right)^2 = k_a \left(\frac{\Delta a}{a}\right)^2 + k_e (\Delta e)^2 + k_i (\Delta \sin i)^2 + k_\Omega (\Delta \Omega)^2 + k_\varpi (\Delta \varpi)^2, \quad (4)$$

with Δa , Δe , $\Delta \sin i$, $\Delta \Omega$, and $\Delta \varpi$ as the difference in semi-major axis, eccentricity, sine of inclination, longitude of the ascending node, and argument of perihelion, respectively; n and a are the mean motion and semi-major axis of either component; and the numerical constants are $k_a = 5/4$, $k_e = k_i = 2$, and $k_\Omega = k_\varpi = 10^{-4}$ ([Pravec et al., 2019](#)). Backward integration has confirmed many of these pairs, with recent epochs in the past during which the two components were within their Hill sphere (see [Žižka et al., 2016](#), for instance). These epochs are considered the ages of the pairs, the time at which the two components became gravitationally unbound.

We consider all the pairs listed in the different sources compiled in the dataCloud. However, for the determination of the age, for the ssoCard we select the most recent determination over older studies.

4.2.5. Diameter

There are a number different methods available to estimate the diameter of a SSO. As a general scheme, we favor estimates obtained by a space mission (either via flyby or rendez-vous, such as [Belton et al., 1992](#)) over all the others. Diameter estimates based on full 3D shape modeling (including direct measurement such as radar echoes, disk-resolved imaging, or stellar occultation) are then considered the most reliable (e.g., [Hudson & Os-](#)

[tro, 1994](#); [Carry et al., 2010](#); [Viikinkoski et al., 2015](#); [Bartczak & Dudziński, 2018](#)).

The next category of methods are convex shape models (generally obtained with the light-curve inversion method, [Kaasalainen & Torppa, 2001](#)) scaled a posteriori using another measurement (stellar occultation or mid-infrared flux, [Durech et al., 2011](#); [Lagerros, 1996](#)) or tri-axial ellipsoid (e.g., [Drummond & Cocke, 1989](#); [Drummond et al., 2014](#)). These are followed by direct measurements limited to a single geometry, such as direct imaging ([Marchis et al., 2006](#)), stellar occultations ([Dunham & Mallen, 1979](#)), interferometry ([Delbo et al., 2009](#)), and broadening of the instrument point-spread function ([Brown & Trujillo, 2004](#)).

Then come the estimates from the analysis of mid-infrared fluxes with spherical models: STM ([Lebofsky et al., 1986](#)), FRM ([Lebofsky & Spencer, 1989](#)), NEATM ([Harris & Davies, 1999](#)), and NESTM ([Wolters & Green, 2009](#)). The last ones chosen are the diameter estimates based on the absolute magnitude, H , and the albedo, p_V , (Section 4.2.6) when the latter has been derived from the polarimetric phase curve of the SSO (e.g., [Delbò et al., 2007](#)). We present the complete list of methods and their order for computing the best diameter estimate in [Table C.1](#).

4.2.6. Albedo

In most cases, the albedo is derived by combining a diameter estimate (D) with the absolute magnitude, H , at visible wavelengths (more specifically in the Johnson V band, hence, the p_V notation), using the canonical equation ([Bowell et al., 1989](#)):

$$p_V = \left(\frac{1329}{D}\right)^2 10^{-0.4H}. \quad (5)$$

An albedo determination is thus closely linked with a diameter estimate and this is why both quantities are reported in a single table in SsODNet.dataCloud. Because the absolute magnitude is constantly refined with the new photometry associated with the astrometry reported to the MPC, we compute p_V using the latest available absolute magnitude, H , and the best estimate of the diameter (Section 4.2.5) using [Equation 5](#). The uncertainties are computed as:

$$\sigma_{\pm, p_V} = p_V \sqrt{4 \left(\frac{\sigma_{\mp, D}}{D}\right)^2 + (0.4 \ln(10) \sigma_{\mp, H})^2}. \quad (6)$$

Uncertainty on H is seldom provided, and we use a default value of 0.3. The only exceptions to this approach are albedo estimated by space missions or, alternatively, from polarimetric phase curves (see [Table C.2](#)), which are not recomputed. We present the albedo against proper orbital elements in [Figure 4](#).

4.2.7. Masses

The determination of the mass of an SSO relies on measuring the effect of its gravitational attraction on another celestial body: either a spacecraft or another(s) SSO(s). The only exception to this is the mass determination from the detection of Yarkovsky drift ([Chesley et al., 2003](#)).

The precision that can be achieved is strongly dependent on the type of interaction, whether that is with: a spacecraft, a satellite in orbit, or long-distance encounters ([Carry, 2012](#); [Scheeres et al., 2015](#)). We thus favor mass estimates achieved by radio science experiments during spacecraft encounters ([Yeomans et al., 1997](#); [Pätzold et al., 2011](#)). Secondary estimates come from

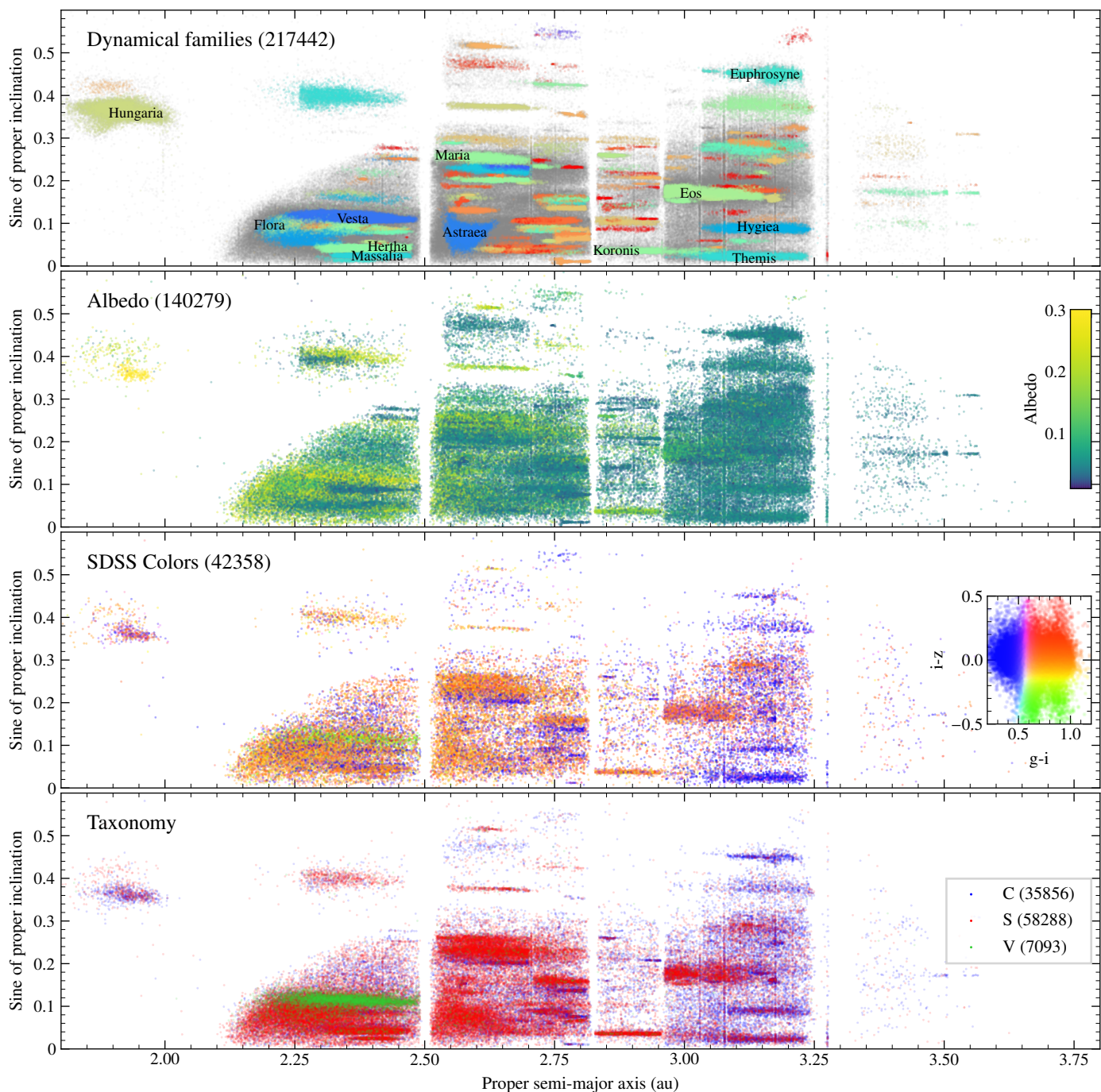


Fig. 4: Distribution of families (first panel), albedo (second), colors (third, using a color-scheme similar to Parker et al. (2008) based on a code by Ivezić et al. (2014)), and taxonomy (fourth) against proper elements (semi-major axis and sine of inclination). The number of plotted objects is reported in each panel.

masses determined in binary systems by studying the orbits of their moons (Merline et al., 1999; Pravec et al., 2000; Ostro et al., 2006; Vachier et al., 2012; Pajuelo et al., 2018).

Masses determined from SSO-to-SSO long-distance interactions: close encounters (Standish & Hellings, 1989; Sitala & Granvik, 2020) and ephemerides (Baer & Chesley, 2008; Fienga et al., 2008) follow. Finally, for an SSO with a detected Yarkovsky drift (Vokrouhlický et al., 2015), it is possible to determine its mass on the basis of a number of other parameters (diameter, albedo, obliquity, thermal inertia, etc., as per Chesley

et al., 2014). We present the complete ordered list of methods for computing the best mass estimate in Table C.3.

4.2.8. Density

For each SSO with both a mass M and a diameter D estimates, we compute its density ρ (kg.m^{-3}) and associated uncertainties

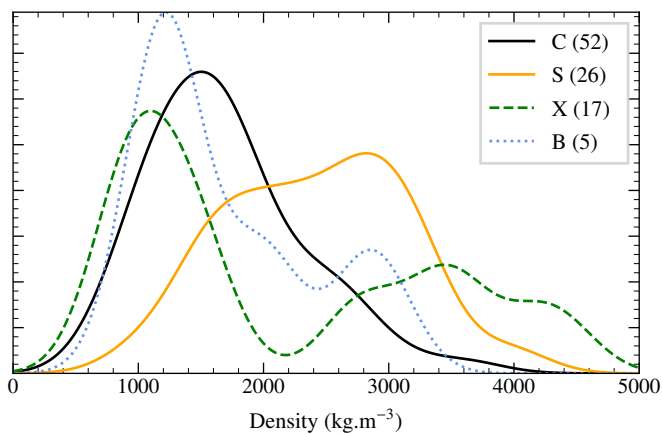


Fig. 5: Kernel density estimate (KDE) of the density of the C, S, X, and B complexes. The bimodal distribution of X-types highlights the P and M sub-classes (average p_V of 0.044 and 0.129, below and above 2000 kg.m^{-3} , respectively). Similarly, Pallas is the sole contributor to high-density B-types.

as follows:

$$\rho = M \sqrt[3]{\frac{\pi}{6} D^3} \quad (7)$$

$$\sigma_{\pm, \rho} = \rho \sqrt{9 \left(\frac{\sigma_{\pm, D}}{D} \right)^2 + \left(\frac{\sigma_{\pm, M}}{M} \right)^2} \quad (8)$$

In some cases, the density can be determined without knowledge of either the mass or the volume. This is often the case of small binary asteroid systems studied by optical light curves (Scheirich & Pravec, 2009; Carry et al., 2015). A few binary systems imaged by radar are also included in this case (Ford et al., 2014). Last, the density can be derived from a detected Yarkovsky orbital drift (Rozitis & Green, 2014). We did not set preference of a method over another and we chose to average these estimates together. The distribution of density for a few selected taxonomic classes is presented in Figure 5.

4.2.9. Spin solutions

In most cases, the only available information on the spin of an SSO is its rotation period (often reported as synodic period). In some cases, however, the orientation of the spin axis has been determined, and we report its coordinates both in ECI2000 (as reference time, longitude, and latitude; see Kaasalainen & Torppa, 2001; Āurech et al., 2010) and in EQJ2000 (as right ascension, declination, and the position of the prime meridian W_0 and \dot{W} ; see Archinal et al., 2018).

Spin-vector coordinates determined with the light-curve inversion method (Kaasalainen & Torppa, 2001) are often degenerated with a mirror solution separated by 180° in ecliptic longitude. We use the selection flag (Section 3) to remove this ambiguity whenever one of the two spin solutions has been rejected a posteriori (from comparison with stellar occultation or disk-resolved imaging for instance, Marchis et al., 2006; Āurech et al., 2011). For each SSO with spin-vector coordinates, we computed its obliquity using these coordinates and its osculating elements (Section 4.2.1). We present the distribution of rotation period and obliquity against diameter in Figure 6.

Here, again, solutions obtained by spacecraft encounters are favored over any others. They are followed by spin solutions obtained by 3D shape modeling techniques that include direct disk-

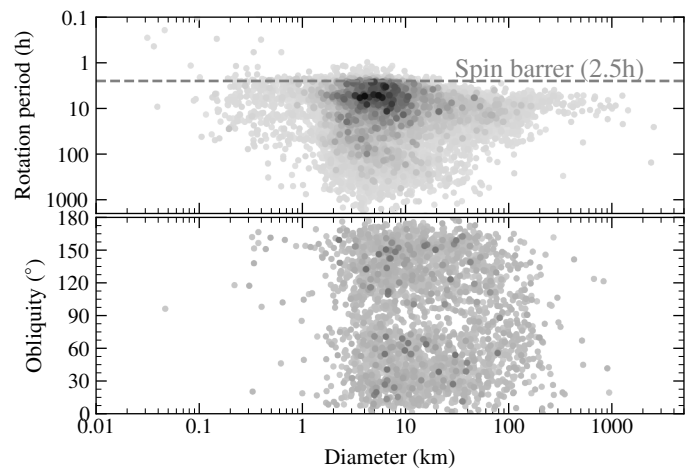


Fig. 6: Rotation period (top) and obliquity (bottom) vs diameter for 17,201 and 2596 SSOs, respectively. Darker shades of grey indicate higher density of points.

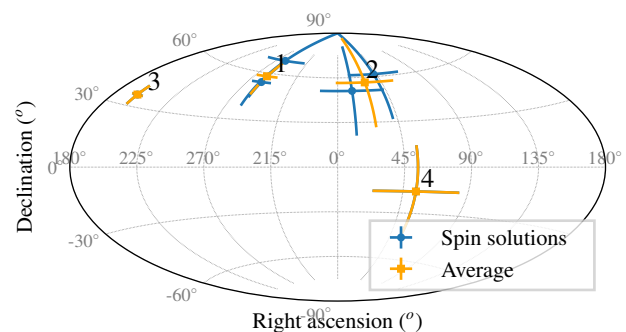


Fig. 7: Example of clustering of spin coordinates for (20) *Massalia*. Six solutions (blue) are possible (Kaasalainen et al., 2002; Hanuš et al., 2016; Cellino et al., 2019). The four separated spin coordinates (orange) of the four clusters are reported in the ssoCard.

resolved measurements (stellar occultations, disk-resolved images, etc., e.g., Tanga et al., 2015; Vernazza et al., 2018; Shepard et al., 2018; Carry et al., 2019). These are followed by 3D shape models that are later scaled using complementary observations (mid-infrared fluxes, stellar occultations, disk-resolved images, etc., Hanuš et al., 2013b; Āurech et al., 2011). Spin solutions associated with convex shape models, generally with a mirrored spin solution, were then chosen (Hanus et al., 2013a; Marciniak et al., 2018), followed by solutions obtained from tri-axial ellipsoids (Drummond & Cocke, 1989; Merline et al., 2013). Finally, there are the periods determined from light curves, with or without constraints on the spin coordinates (Lagerkvist, 1978; Yeh et al., 2020). We refer to Table C.4 for a full listing of the order of preference.

The average spin coordinates are computed using Equation 1. However, as several ambiguous spin solutions may coexist for a given SSO, we identify which estimates correspond to which spin solution using K-Means clustering (Lloyd, 1982), as provided by the `scikit-learn`²¹ python package (Pedregosa et al., 2011). We consider that up to four distinct spin solutions can be present, such as for (20) *Massalia* (Figure 7). Spin coordinates must be within 30° of the average to be include in a cluster.

²¹ <https://scikit-learn.org>

We set default uncertainties of 30° on spin coordinates whenever they have not been specified by the respective authors. We used a similar approach, based on K-Means clustering, for the rotation periods. In this case, the threshold to belong to a solution was set to 0.2 h. The default uncertainty was set to 1 h.

4.2.10. Colors

Stricto sensu, the colors of SSOs are observable and not derived properties. Nevertheless, we compiled the colors of SSOs in SsODNet.dataCloud, with the same rationale as for derived properties: many colors are available but spread over many studies (e.g., Dandy et al., 2003; Snodgrass et al., 2010; Dumitru et al., 2018) and they are usually not in machine-readable format. Furthermore, colors can be used for taxonomic determination (Carvano et al., 2010; DeMeo & Carry, 2013).

Several ancillary information for contextualization are recorded (Table A.3), such as the observing time, the source of measurement (plain English description and IAU Observatory code²² if available). The filters used to compute the colors are identified with the unique identifier of the SVO Filter Service²³ providing transmission curves and zero points (Rodrigo et al., 2012; Rodrigo & Solano, 2020). Similarly, we record in which system the photometry is reported (Vega, AB, or ST).

The selection of best estimates is based on the time difference, Δ_t , between the observation of the two filters and how the color was computed. We favor (Table C.5) colors computed as a difference of absolute magnitudes from phase functions in each filter (Mahlke et al., 2021; Alvarez-Candal et al., 2021). In that case, we report the most-recent published value. Then we follow up with the colors computed as a difference of apparent magnitudes but corrected for light curve variations (Mommert et al., 2016; Erasmus et al., 2019). Last, we have the simple difference of apparent magnitudes (Popescu et al., 2018; Sergeev & Carry, 2021). Whenever several estimates of the same color with the two latter methods are reported, we computed their average as in Equation 1, with the following weight to account for time difference: $w_i = 1/\sigma_i^2 + 1/\Delta_t^2$. Whenever the information on Δ_t is missing, we set it to 1 h.

Last but not least, filter transmissions are different in each facility. For a given color (e.g., $g-i$), the values from different observatories may differ (e.g., between the Sloan Digital Sky Survey and SkyMapper, see Fig. 9 in Sergeev et al., 2022). We did not merge colors obtained with different filter sets, for instance, SLOAN/SDSS ($g-i$) vs. SkyMapper/SkyMapper ($g-i$), but instead we report the most precise results. An example of these colors is shown in Figure 4.

4.2.11. Phase function

Phase functions describe the evolution of brightness with the phase angle (once it is corrected with respect to the Sun-target and target-observer distances). The absolute magnitude reported together with osculating elements (Section 4.2.1) is computed using the historical two-parameter HG phase function (Bowell et al., 1989), where G is generally assumed to be 0.15. This function has been shown to deviate from observed photometry at low and high phase angle, and a three-parameter HG₁G₂ function has been proposed (Muinonen et al., 2010). We collect these parameters in the dataCloud and report them in ssoCard. Because

²² <https://minorplanetcenter.net/iau/lists/ObsCodesF.html>

²³ <http://svo2.cab.inta-csic.es/theory/fps/>

phase functions are wavelength-dependent (Sanchez et al., 2012; Mahlke et al., 2021), we associate these parameters with the filter in which they were derived, again using the unique identifier of the SVO Filter Service (Rodrigo et al., 2012; Rodrigo & Solano, 2020).

A parameterized version of the phase function has been proposed for low-accuracy data (with two parameters, HG₁₂, later refined as HG₁₂^{*}, Penttilä et al., 2016). However, we stick to HG₁G₂ parameters only, as they have been shown to convey taxonomic and albedo information (Shevchenko et al., 2016; Mahlke et al., 2021).

4.2.12. Taxonomy

Taxonomy is often used as a proxy for composition in statistical studies of populations (Parker et al., 2008; DeMeo & Carry, 2014; Binzel et al., 2019; Hasegawa et al., 2021). The complexity of compiling taxonomic classes is manifold. First, several taxonomies (as classification schemes) have been developed and used by the community, such as Tedesco et al. (1989), Tholen (1989), Bus & Binzel (2002), DeMeo et al. (2009), and Mahlke et al. (2022). Second, there is a great diversity in the potential combinations of these schemes with observing techniques (multi-filter photometry and spectroscopy, Xu et al., 1995; Carry et al., 2016) and wavelength (visible only, near-infrared only, and both, Carvano et al., 2010; Popescu et al., 2018; Marsset et al., 2014).

We present in Figure 8 the decision tree we applied to select the most relevant taxonomy for a given SSO. As a general rule, results from spectroscopy are favored over results from multi-filter photometry. Within each observing technique, the results using both visible and near-infrared are favored, then those based on infrared only, and then finally those based on the visible only. Once the observing technique and wavelength range is selected, there may be several taxonomic schemes available, and we chose the Mahlke, Bus-DeMeo, SMASS, Bus, and Tholen taxonomies, respectively.

In an attempt to homogenize all the classes that have been reported for a given object, we also group similar classes under the term “complex,” following the associations listed in Table C.8. We give an example of the orbital distribution of these complexes in Figure 4.

4.2.13. Thermal properties

Mid-infrared fluxes are often used to determine the diameter of an SSO (Section 4.2.5), from simple thermal models such as NEATM (Harris & Davies, 1999). More complex thermal models (referred to as thermophysical models, TPM, Lagerros, 1996) can also be used, but require additional information on the object such as spin, 3D shape, and so on. One parameter used in TPM is the thermal inertia (in $\text{J}\cdot\text{s}^{-1/2}\cdot\text{K}^{-1}\cdot\text{m}^{-2}$) controlling the resistance of the surface to changes of temperature.

The thermal inertia determination from spacecrafts are favored (Capria et al., 2014), followed by those determined from TPM using a priori knowledge on the spin and shape (Matter et al., 2013; O’Rourke et al., 2012), and, finally, the TPM applied to spheres (Müller et al., 2013), as listed in Table C.6. Thermal inertia (Γ) is a function of heliocentric distance (Vasavada et al., 1999; Rozitis et al., 2018). We thus report the thermal inertia at 1 au (Γ_0) from the Sun in the ssoCard, using the following relation:

$$\Gamma = \Gamma_0 r_H^\alpha, \quad (9)$$

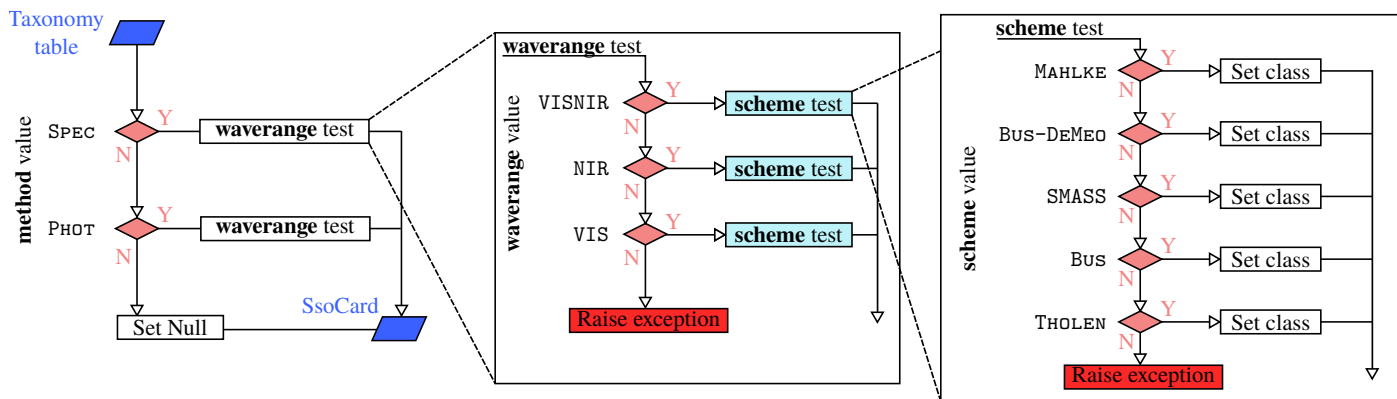


Fig. 8: Decision tree for taxonomic classes. Classes based on spectroscopy are favored upon those based on broad-band photometry only. Similarly data sets covering the full VISNIR wavelength range are favored over NIR only, itself preferred to VIS only. Finally, for classification based on similar data sets, the Muhlke scheme is preferred over Bus-DeMeo, Bus, SMASS, and Tholen schemes.

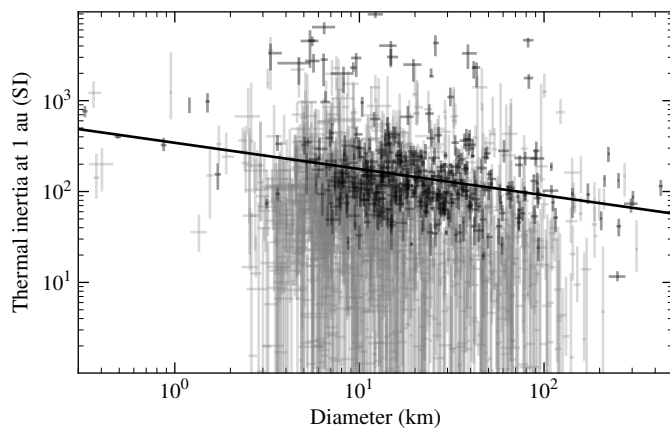


Fig. 9: All 1681 SSOs with a thermal inertia above 1 SI (gray), the 419 with a S/N above 3 (black), and a linear regression on the latter of equation $\log(\Gamma_0) = 2.5 - 0.29 \log(D)$, a result that is similar to the recent work of Hung et al. (2022).

where r_H is the heliocentric distance at the time of the observations and we take $\alpha = -3/4$ following Delbo et al. (2015). We present the distribution of thermal inertia against diameter in Figure 9.

4.2.14. Yarkovsky drift

While the orbital drift due to the delayed thermal emission by asteroid surface is extremely small (of the order of 10^{-4} au/Myr, Vokrouhlický et al., 2015), it was detected for the first time almost two decades ago (Chesley et al., 2003). We favor detections that include both optical and radar observations (Farnocchia et al., 2014, for instance) over those using optical only (e.g., Del Vigna et al., 2018). Finally, we consider those (Table C.7) estimated based on the age of dynamical families (Carruba et al., 2017).

Some authors have reported the semi-major axis drift, \dot{a} (Nugent et al., 2012), while others have given the transverse acceleration, A_2 (Greenstreet et al., 2019), as in the case of cometary dynamical models (Marsden et al., 1973). We report both parameters in the ssoCard, using the following equation from Farnoc-

chia et al. (2013) to convert between quantities:

$$\dot{a} = \frac{A_2}{a^2(1-e^2)\pi n} \int_0^{2\pi} (1 + e \cos f) df, \quad (10)$$

with a as the semi-major axis, e as the eccentricity, and n as the mean motion (Section 4.2.1).

5. Summary for all SSOs: ssoBFT

The ssoCard service described in previous section provides convenient access to the best estimates of many parameters, but limited to a single SSO. The last service composing SsODNet thus provides a broad and flat table (ssoBFT) that compiles all the parameters of the ssoCard for all SSOs. This table is very large (over 591 fields for 1 223 984 SSOs, about 2.1 Gb). Yet, most fields are empty (i.e., there is no estimate of the given parameter for this SSO), resulting in only a 14.6% filling factor.

We propose the ssoBFT as an enhanced character separated values (eCSV²⁴) and an Apache parquet²⁵ files for users interested in the statistical properties of the asteroid population. These files can be downloaded at static urls (eCSV²⁶, parquet²⁷). We also provide this table to the CDS to ensure its fully VO-compliant access.

6. Accessing the services: SsODNet & rocks

We offer several access interfaces to the SsODNet service, described below.

6.1. REST interface

The quero representational state transfer (REST) API is a low-level interface dedicated to developers. It is designed to offer an easy-to-use and fast solution to search for planetary objects (sso and search methods) to resolve their designations (resolver method) or to be used as an auto-completion mechanism for names (instant search method) into Web forms and applications connected to the Internet. In the framework of the Virtual

²⁴ <https://github.com/astropy/astropy-APes/blob/main/APE6.rst>

²⁵ <https://parquet.apache.org/>

²⁶ <https://ssp.imcce.fr/data/ssoBFT-latest.ecsv.bz2>

²⁷ <https://ssp.imcce.fr/data/ssoBFT-latest.parquet>

Observatory, no standard protocol nor technical specification is quite capable of designing a fast-search engine. Thus, the core of SsODNet name resolver does not follow any current VO standard. Nevertheless, the underlying technology and the API we have chosen being intrinsically interoperable, the quaero service can easily be included in any VO ecosystem.

End-point: <https://api.ssodnet.imcce.fr/quaero/1/>
 Doc: <https://doc.ssodnet.imcce.fr/quaero.html>

6.2. Web-service interface

We provide a Web-service interface, built upon XML and SOAP technology, that allows for a full interaction with SsODNet through several methods: (i) `resolver`: to identify SSO (high level API), (ii) `datacloud`: to retrieve all known values of SSO properties, (iii) `ssocard`: to retrieve the best estimates of SSO properties. The user can simply post a request to the method endpoints to gather corresponding data, using a data transfer program such as `wget` or `curl`. More advanced users can implement the SOAP Web service to ensure an application-to-application communication between SsODNet and a software or a public Web page.

SsODNet server: <https://ssp.imcce.fr/webservices/ssodnet/ssodnet.php>
 Public interface: <https://ssp.imcce.fr/webservices/ssodnet/ssodnet.php?wsdl>
 Doc: <https://ssp.imcce.fr/webservices/ssodnet/>

6.3. Web form interface

The easiest way to search for a SSO and to quickly consult its properties may be to use SsODNet dedicated Web form. The best estimates of the physical and dynamic properties (the `ssoCard`) are displayed in a comprehensive manner, together with bibliographic references. We also provide links to all values (i.e., `dataCloud` entry for each property of the SSO), and to the subset used to compute the best estimates (as defined by the decision trees, see Section 4).

Web form: <https://ssp.imcce.fr/forms/ssocard/>
 Doc: <https://ssp.imcce.fr/forms/ssocard/doc>

6.4. Python interface: `rocks`

We provide a `python` interface to SsODNet named `rocks`. It offers a programmatic entry point both for data exploration and data processing. The interaction with the SsODNet repositories is asynchronous and results are cached on the user-side, providing a responsive user experience.

Sources: <https://github.com/maxmahlke/rocks>
 Doc: <https://rocks.readthedocs.io>

Data exploration is accessible via the command line interface of `rocks` in a straightforward, uniform syntax:

```
$ rocks [command|parameter] [asteroid_identifier]
```

Here, the `parameter` can be any key from the `ssoCard` or `dataCloud` catalogs, while the `asteroid_identifier` is any identifier that can be resolved by `quaero`. The result of the query is printed in the console. Commands such as `id` and `info` serve to identify an asteroid and to print the asteroid's `ssoCard`.

```
$ rocks id "1975 XP"
(234) Barbara
$ rocks taxonomy Barbara
L
$ rocks diameter barbara
46.3 +- 5.0 km
$ rocks albedo 234
0.187 +- 0.2839
```

An overview of all compiled literature values is printed when requesting the plural of the parameters. This is possible for all parameters which have `dataCloud` entries, such as `albedo`, `mass`, `taxonomy`, etc.

```
$ rocks taxonomies ceres
+-----+-----+-----+-----+
| class | method | scheme | shortbib |
+-----+-----+-----+-----+
| G      | Phot    | Tholen | Tholen+1989 |
| C      | Spec    | Bus    | Bus&Binzel+2002 |
| C      | Spec    | Bus    | Lazzaro+2004 |
| C      | Spec    | Tholen | Lazzaro+2004 |
| C      | Spec    | Bus-DeMeo | DeMeo+2009 |
| C      | Spec    | Bus    | Fornasier+2014b |
| G      | Spec    | Tholen | Fornasier+2014b |
| C      | Phot    | Bus-DeMeo | Sergejev+2022 |
| C      | Spec    | Mahlke | Mahlke+2022 |
+-----+-----+-----+-----+
```

Data processing is facilitated for `python` scripts using the `rocks` package. The main entry point is the `rocks.Rock` class, where each instance reflects a unique asteroid. The asteroid parameters are accessible as class attributes via the dot notation, which again leads to an intuitive syntax:

```
>>> import rocks
>>> vesta = rocks.Rock(4)
>>> vesta.albedo.value
0.38
>>> vesta.albedo.error.min_
-0.04
>>> vesta.albedo.error.max_
0.04
>>> vesta.albedo.description
'Geometrical albedo in V band'
```

The asynchronous interaction with the locally cached data and the remote SsODNet repositories allow for a fast analysis process without the use of resource-intensive multiprocessing or multi-threading strategies. To provide an estimate of the execution times, we identified all asteroids in the SDSS Moving Object Catalog DR1²⁸ and retrieved their `ssoCard`. The catalog contains observations of 10,585 unique minor bodies, largely

²⁸ <http://faculty.washington.edu/ivezic/sdssmoc/sdssmoc.html>

referred to by designations that are no longer the main identifier of the object. Using a combination of `quaero` queries and a local asteroid name-number-designation index, `rocks` identifies all objects within 2.5 s. The `ssoCards` are retrieved within 320 s from `SsODNet`, about 30 ms per asteroid. `rocks` then performs data validation and deserialization (i.e., converting the JSON server response into a `python` object) within 120 s, that is, about 11 ms per asteroid. A second execution of the analysis script would benefit from the locally cached `ssoCards`, rendering any request to `SsODNet` obsolete.

To install `rocks`, we can use the `python` package index (PyPI) under the package name `space-rocks`. The online documentation²⁹ provides a guide on getting started and tutorials to achieve more advanced data processing results. We note that `rocks` is actively developed and maintained by the authors of this work.

7. Future developments

We foresee several lines of development for the `SsODNet` service: data compilation and curation, expansion of the set of parameters and types of SSOs, and development of the interface.

Data compilation: First and foremost, we will continue to compile data into the `dataCloud`, aiming for completeness with respect to the listed parameters. Indeed, it is the building block of the `ssoCard` and the `ssoBFT`, which are automatically generated from the entries in the `dataCloud`. On the other hand, `quaero` has been working and been updated weekly for several years, following the growing list of SSOs listed by the MPC. Thus, a continuous scientific monitoring of publications is required for the service.

We welcome any feedback, especially on data sources that may be missing or erroneous entries. While we conducted multiple checks on the data included in `SsODNet`, some typographical errors may lurk in the unprecedented size of the data compilation. We will happily include sources that are not included in the current release of the service and correct entries.

Furthermore, `SsODNet` can be used by any group or researcher to publish regularly updated data. A simple file (VOTable, csv, ...), with sufficient metadata at a static url can be used as a source, without requiring a server or a database with a web service.

Set of parameters: The set of parameters currently available in `SsODNet` is already broad, covering dynamical, surface, and physical properties (Table A.1). There are, however, other parameters of interest that will be added to the `dataCloud` (and, hence, `ssoCard` and `ssoBFT`), such as the source region probabilities for near-Earth objects (Granvik et al., 2017) and their minimal orbital intersection distance with planets (MOID, Marsden, 1993), activity for asteroids and Centaurs (Hsieh & Jewitt, 2006; Jewitt, 2009), and radar albedos (Neeley et al., 2014). Additional computed parameters can also be added in `ssoCard`, such as surface gravity or escape velocity.

Types of SSOs: The present release of `SsODNet` focuses on asteroids because they are the prime targets of study of the authors. The service was nevertheless designed to cope with all classes of

SSOs: comets, planets, satellites, and interstellar objects. For instance, `quaero` already deals with the designation of all these categories.

We thus welcome partnership with everyone willing to contribute to build this community database. Beside the collection and curation of data, a set of parameters relevant for these celestial bodies must be defined (e.g., non-gravitational acceleration for comets, libration amplitude and frequency for satellites), together with decision trees to estimate the best parameters. `SsODNet` has been envisioned as a service to the community and any contribution to it will expand its advantages.

User interface: `SsODNet` is mainly a machine-machine service, allowing for on-the-fly data retrieval. Both `quaero` and `ssoCard` are designed to cope with constant queries. The `dataCloud` entries for a given SSO can also be dumped easily, and the `ssoBFT` downloaded as a whole.

We plan to develop more advanced possibilities to query the data, both in `dataCloud` and `ssoBFT`. Users may be interested by searching entries from a given bibliographic reference, rather than for a specific SSO for instance. Similarly, users may be interested in a subset of the `ssoBFT` only (e.g., some specific parameters only for SSOs fulfilling certain conditions). While the latter is possible with TAP on the version of the `ssoBFT` hosted at the CDS, the former requires development on the server side of `SsODNet`.

8. Conclusions

We present a new Web Service, `SsODNet`, which provides a convenient solution to the issues of SSO identification and the compilation of properties. It consists of a suite of applications, each with its own programming interface: `quaero` for name resolution, `dataCloud` compiling SSO properties, `ssoCard` providing the set of best estimates for each SSO, and `ssoBFT` compiling the latter for all SSOs. These entry points deliver JSON as native outputs. We have released a `python` interface for these services: `rocks`, available in the `python` package index (PyPI). `SsODNet` is fully operational. The name resolver `quaero` is updated weekly to follow SSO discoveries. We plan on monthly updates for the others applications, following compilation of data from continuous monitoring of new publications. The future evolution of the service includes an extension of the suite of properties and classes of SSOs, along with an advanced query interface to retrieve large corpus of data.

Acknowledgements. This research has made use of the SVO Filter Profile Service supported from the Spanish MINECO through grant AYA2017-84089 (Rodrigo et al., 2012; Rodrigo & Solano, 2020). This research has made use of the `scikit-learn` `python` package (Pedregosa et al., 2011). We did an extensive use of the VO TOPCAT software (Taylor, 2005). Thanks to all the developers and maintainers. We would like to thank J. Masiero, F. E. DeMeo, and F. Spoto for discussions that led to the current decision trees used in `SsODNet`.

References

- Ahn, C. P., Alexandroff, R., Allende Prieto, C., et al. 2012, *ApJS*, 203, 21
- Alvarez-Candal, A., Benavidez, P. G., Campo Bagatin, A., & Santana-Ros, T. 2021, arXiv e-prints, arXiv:2110.06621
- Archinal, B. A., Acton, C. H., A'Hearn, M. F., et al. 2018, *Celestial Mechanics and Dynamical Astronomy*, 130, 22
- Baer, J. & Chesley, S. R. 2008, *Celestial Mechanics and Dynamical Astronomy*, 100, 27
- Bailey, S. I. & Pickering, E. C. 1913, *Annals of Harvard College Observatory*, 72, 165
- Bartczak, P. & Dudziński, G. 2018, *MNRAS*, 473, 5050

²⁹ <https://rocks.readthedocs.io>

- Bayo, A., Rodrigo, C., Barrado Y Navascués, D., et al. 2008, *A&A*, 492, 277
- Bell, J. F., Owensby, P. D., Hawke, B. R., & Gaffey, M. J. 1988, in *Lunar and Planetary Science Conference*, Vol. 19, Lunar and Planetary Science Conference, 57
- Belskaya, I. N. & Shevchenko, V. G. 2000, *Icarus*, 147, 94
- Belton, M. J. S., Veverka, J., Thomas, P., et al. 1992, *Science*, 257, 1647
- Berthier, J., Hestroffer, D., Carry, B., et al. 2008, *LPI Contributions*, 1405, 8374
- Berthier, J., Vachier, F., Thuillot, W., et al. 2006, in *Astronomical Society of the Pacific Conference Series*, Vol. 351, *Astronomical Data Analysis Software and Systems XV*, ed. C. Gabriel, C. Arviset, D. Ponz, & S. Enrique, 367–+
- Binzel, R. P., DeMeo, F. E., Turtelboom, E. V., et al. 2019, *Icarus*, 324, 41
- Binzel, R. P., Xu, S., Bus, S. J., et al. 1993, *Science*, 262, 1541
- Bolin, B. T., Delbo, M., Morbidelli, A., & Walsh, K. J. 2017, *Icarus*, 282, 290
- Bowell, E., Chapman, C. R., Gradie, J. C., Morrison, D., & Zellner, B. 1978, *Icarus*, 35, 313
- Bowell, E., Hapke, B., Domingue, D., et al. 1989, *Asteroids II*, 524
- Bowell, E., Muinonen, K., & Wasserman, L. H. 1994, in *Asteroids, Comets, Meteors 1993*, ed. A. Milani, M. di Martino, & A. Cellino, Vol. 160, 477–481
- Bray, T., E. 2017
- Brown, M. E. & Trujillo, C. A. 2004, *AJ*, 127, 2413
- Bus, S. J. & Binzel, R. P. 2002, *Icarus*, 158, 146
- Capria, M. T., Tosi, F., De Sanctis, M. C., et al. 2014, *Geophys. Res. Lett.*, 41, 1438
- Carruba, V., Vokrouhlický, D., & Nesvorný, D. 2017, *MNRAS*, 469, 4400
- Carry, B. 2012, *Planet. Space Sci.*, 73, 98
- Carry, B., Dumas, C., Kaasalainen, M., et al. 2010, *Icarus*, 205, 460
- Carry, B., Matter, A., Scheirich, P., et al. 2015, *Icarus*, 248, 516
- Carry, B., Solano, E., Eggl, S., & DeMeo, F. E. 2016, *Icarus*, 268, 340
- Carry, B., Vachier, F., Berthier, J., et al. 2019, *A&A*, 623, A132
- Carvano, J. M., Hasselmann, P. H., Lazzaro, D., & Mothé-Diniz, T. 2010, *A&A*, 510, A43
- Cellino, A., Hestroffer, D., Lu, X. P., Muinonen, K., & Tanga, P. 2019, *A&A*, 631, A67
- Cellino, A., Hutton, R. G., Tedesco, E. F., Di Martino, M., & Brunini, A. 1999, *Icarus*, 138, 129
- Chapman, C. R., Morrison, D., & Zellner, B. 1975, *Icarus*, 25, 104
- Chesley, S. R., Farnocchia, D., Nolan, M. C., et al. 2014, *Icarus*, 235, 5
- Chesley, S. R., Ostro, S. J., Vokrouhlický, D., et al. 2003, *Science*, 302, 1739
- Cruikshank, D. P. & Morrison, D. 1973, *Icarus*, 20, 477
- Cutri, R. M., Wright, E. L., Conrow, T., et al. 2013, *Explanatory Supplement to the AllWISE Data Release Products*, *Explanatory Supplement to the AllWISE Data Release Products*
- Dandy, C. L., Fitzsimmons, A., & Collander-Brown, S. J. 2003, *Icarus*, 163, 363
- Davidsson, B. J. R., Gutiérrez, P. J., & Rickman, H. 2007, *Icarus*, 187, 306
- Del Vigna, A., Faggioli, L., Milani, A., et al. 2018, *A&A*, 617, A61
- Del Vigna, A., Roa, J., Farnocchia, D., et al. 2019, *A&A*, 627, L11
- Delbo, M., Avdellidou, C., & Morbidelli, A. 2019, *A&A*, 624, A69
- Delbò, M., Cellino, A., & Tedesco, E. F. 2007, *Icarus*, 188, 266
- Delbo, M., Ligorì, S., Matter, A., Cellino, A., & Berthier, J. 2009, *ApJ*, 694, 1228
- Delbo, M., Mueller, M., Emery, J. P., Rozitis, B., & Capria, M. T. 2015, *Asteroid Thermophysical Modeling*, 107–128
- Delbo, M., Tanga, P., Carry, B., Ordenovic, C., & Bottein, P. 2018, in *Asteroids, Comets, and Meteors*: ACM 2018
- DeMeo, F. E., Binzel, R. P., Slivan, S. M., & Bus, S. J. 2009, *Icarus*, 202, 160
- DeMeo, F. E. & Carry, B. 2013, *Icarus*, 226, 723
- DeMeo, F. E. & Carry, B. 2014, *Nature*, 505, 629
- Devogèle, M., Moskovitz, N., Thirouin, A., et al. 2019, *AJ*, 158, 196
- Drummond, J. D. 2000, in *NATO Advanced Study Institute (ASI) Series C*, Vol. 551, *Laser Guide Star Adaptive Optics for Astronomy*, ed. N. Ageorges & C. Dainty, 243
- Drummond, J. D., Carry, B., Merline, W. J., et al. 2014, *Icarus*, 236, 28
- Drummond, J. D. & Cocke, W. J. 1989, *Icarus*, 78, 323
- Drummond, J. D., Cocke, W. J., Hege, E. K., & Strittmatter, P. A. 1985, *Icarus*, 61, 132
- Dumitru, B. A., Birlan, M., Sonka, A., Colas, F., & Nedelcu, D. A. 2018, *Astronomische Nachrichten*, 339, 198
- Dunham, D. W. & Mallen, G. 1979, *Rev. Mexicana Astron. Astrofis.*, 4, 205
- Đurech, J., Sidorin, V., & Kaasalainen, M. 2010, *A&A*, 513, A46
- Erasmus, N., McNeill, A., Mommert, M., et al. 2019, *ApJS*, 242, 15
- Exoplanet-Team. 2021, *The Extrasolar Planets Encyclopaedia*, <http://www.exoplanet.eu/>
- Farnocchia, D., Chesley, S. R., Tholen, D. J., & Micheli, M. 2014, *Celestial Mechanics and Dynamical Astronomy*, 119, 301
- Farnocchia, D., Chesley, S. R., Vokrouhlický, D., et al. 2013, *Icarus*, 224, 1
- Fenucci, M., Novaković, B., Vokrouhlický, D., & Weryk, R. J. 2021, *A&A*, 647, A61
- Fienga, A., Manche, H., Laskar, J., & Gastineau, M. 2008, *A&A*, 477, 315
- Ford, T. F., Benner, L. A., Brozovic, M., et al. 2014, in *AAS/Division for Planetary Sciences Meeting Abstracts*, Vol. 46, *AAS/Division for Planetary Sciences Meeting Abstracts #46*, 213.15
- Gaia Collaboration, Brown, A. G. A., Vallenari, A., et al. 2018, *A&A*, 616, A1
- Gaia Collaboration, Brown, A. G. A., Vallenari, A., et al. 2021, *A&A*, 649, A1
- Gaia Collaboration, Brown, A. G. A., Vallenari, A., et al. 2016, *A&A*, 595, A2
- Gauss, K. F. 1809, *Theoria motvs corporvm coelestivm in sectionibvs conicis solem ambientivm*.
- Gehrels, T. 1956, *ApJ*, 123, 331
- Gradie, J. & Tedesco, E. 1982, *Science*, 216, 1405
- Granvik, M., Morbidelli, A., Vokrouhlický, D., et al. 2017, *A&A*, 598, A52
- Grav, T., Mainzer, A. K., Bauer, J., et al. 2011, *ApJ*, 742, 40
- Greenberg, A. H., Margot, J.-L., Verma, A. K., Taylor, P. A., & Hodge, S. E. 2020, *AJ*, 159, 92
- Greenstreet, S., Farnocchia, D., & Lister, T. 2019, *Icarus*, 321, 564
- Hanuš, J., Brož, M., Durech, J., et al. 2013a, *A&A*, 559, A134
- Hanuš, J., Delbo', M., Durech, J., & Alí-Lagoa, V. 2015, *Icarus*, 256, 101
- Hanuš, J., Delbo', M., Durech, J., & Alí-Lagoa, V. 2018, *Icarus*, 309, 297
- Hanuš, J., Marchis, F., & Durech, J. 2013b, *Icarus*, 226, 1045
- Hanuš, J., Pejcha, O., Shappee, B. J., et al. 2021, *A&A*, 654, A48
- Hanuš, J., Durech, J., Oszkiewicz, D. A., et al. 2016, *A&A*, 586, A108
- Harris, A. W. & Davies, J. K. 1999, *Icarus*, 142, 464
- Hasegawa, S., Marsset, M., DeMeo, F. E., et al. 2021, *ApJ*, 916, L6
- Hirayama, K. 1918, *AJ*, 31, 185
- Hsieh, H. H. & Jewitt, D. 2006, *Science*, 312, 561
- Hudson, R. S. & Ostro, S. J. 1994, *Science*, 263, 940
- Hudson, R. S., Ostro, S. J., & Harris, A. W. 1997, *Icarus*, 130, 165
- Hung, D., Hanuš, J., Masiero, J. R., & Tholen, D. J. 2022, *PSJ*, 3, 56
- IAU. 2020a, *Naming of Astronomical Objects*
- IAU. 2020b, *Naming of Exoplanets*
- Ivezić, Ž., Connolly, A., Vanderplas, J., & Gray, A. 2014, *Statistics, Data Mining and Machine Learning in Astronomy* (Princeton University Press)
- Jewitt, D. 2009, *AJ*, 137, 4296
- Kaasalainen, M. & Torppa, J. 2001, *Icarus*, 153, 24
- Kaasalainen, M., Torppa, J., & Piironen, J. 2002, *Icarus*, 159, 369
- Kelso, T. 2021, *CelesTrak*, <https://celestrak.com/>
- Knežević, Z., Lemaître, A., & Milani, A. 2002, *The Determination of Asteroid Proper Elements*, 603–612
- Knežević, Z. & Milani, A. 2000, *Celestial Mechanics and Dynamical Astronomy*, 78, 17
- Knežević, Z. & Milani, A. 2003, *A&A*, 403, 1165
- Knežević, Z. & Milani, A. 2012, in *IAU Joint Discussion*, *IAU Joint Discussion*, P18
- Kovalenko, I., Kempf, J., Popovichenko, O., Gateau, T., & Lizy-Destrez, S. 2022, *Planet. Space Sci.*, 215, 105463
- Kretlow, M. 2020, in *European Planetary Science Congress*, EPSC2020–690
- Lagerkvist, C. I. 1978, *A&AS*, 34, 203
- Lagerros, J. S. V. 1996, *A&A*, 310, 1011
- Lebofsky, L. A. & Spencer, J. R. 1989, in *Asteroids II*, ed. R. P. Binzel, T. Gehrels, & M. S. Matthews, 128–147
- Lebofsky, L. A., Sykes, M. V., Tedesco, E. F., et al. 1986, *Icarus*, 68, 239
- Lister, T. A., Gomez, E., Chatelain, J., et al. 2021, *Icarus*, 364, 114387
- Lloyd, S. 1982, *IEEE Transactions on Information Theory*, 28, 129
- Mahlke, M., Carry, B., & Denneau, L. 2021, *Icarus*, 354, 114094
- Mahlke, M., Carry, B., & Mattei, P.-A. 2022, *arXiv e-prints*, arXiv:2203.11229
- Mainzer, A., Grav, T., Bauer, J., et al. 2011, *ApJ*, 743, 156
- Marchis, F., Kaasalainen, M., Hom, E. F. Y., et al. 2006, *Icarus*, 185, 39
- Marciniak, A., Bartczak, P., Müller, T., et al. 2018, *A&A*, 610, A7
- Marciniak, A., Bartczak, P., Santana-Ros, T., et al. 2012, *A&A*, 545, A131
- Marrese, P. M., Marinoni, S., Fabrizio, M., & Giuffrida, G. 2017, *A&A*, 607, A105
- Marsden, B. G. 1980, *Celestial Mechanics*, 22, 63
- Marsden, B. G. 1993, in *Near-Earth-Objects Interception Workshop*, Vol. 36, *Proceedings of the Near-Earth-Objects Interception Workshop*, ed. G. H. Canavan, J. C. Solem, & J. D. G. Rather, 67–71
- Marsden, B. G., Sekanina, Z., & Yeomans, D. K. 1973, *AJ*, 78, 211
- Marsset, M., Vernazza, P., Gourgeot, F., et al. 2014, *A&A*, 568, L7
- Masiero, J. R., Mainzer, A. K., Bauer, J. M., et al. 2013, *ApJ*, 770, 7
- Masiero, J. R., Mainzer, A. K., Grav, T., et al. 2011, *ApJ*, 741, 68
- Matter, A., Delbo, M., Carry, B., & Ligorì, S. 2013, *Icarus*, 226, 419
- Mayor, M. & Queloz, D. 1995, *Nature*, 378, 355
- McCord, T. B., Adams, J. B., & Johnson, T. V. 1970, *Science*, 168, 1445
- Merline, W. J., Close, L. M., Dumas, C., et al. 1999, *Nature*, 401, 565
- Merline, W. J., Drummond, J. D., Carry, B., et al. 2013, *Icarus*, 225, 794
- Milani, A., Cellino, A., Knežević, Z., et al. 2014, *Icarus*, 239, 46
- Milani, A. & Knežević, Z. 1990, *Celestial Mechanics and Dynamical Astronomy*, 49, 347
- Milani, A. & Knežević, Z. 1994, *Icarus*, 107, 219
- Mommert, M., Trilling, D. E., Borth, D., et al. 2016, *AJ*, 151, 98

- Moskovitz, N., Burt, B., Schottland, R., et al. 2021, in AAS/Division for Planetary Sciences Meeting Abstracts, Vol. 53, AAS/Division for Planetary Sciences Meeting Abstracts, 101.04
- MPC. 2021, MPCAT-OBS: Observation Archive, <https://minorplanetcenter.net/iau/ECS/MPCAT-OBS/MPCAT-OBS.html>
- Mueller, B. E. A., Tholen, D. J., Hartmann, W. K., & Cruikshank, D. P. 1992, *Icarus*, 97, 150
- Muinenen, K., Belskaya, I. N., Cellino, A., et al. 2010, *Icarus*, 209, 542
- Müller, T. G., Miyata, T., Kiss, C., et al. 2013, *A&A*, 558, A97
- Neeley, J. R., Clark, B. E., Ockert-Bell, M. E., et al. 2014, *Icarus*, 238, 37
- Nesvorný, D. 2015, NASA Planetary Data System, EAR
- Newton, I. 1760, *Philosophiae naturalis principia mathematica*, vol. 1 - 4
- Novakovic, B. & Radovic, V. 2019, in EPSC-DPS Joint Meeting 2019, Vol. 2019, EPSC-DPS2019-1671
- Nugent, C. R., Margot, J. L., Chesley, S. R., & Vokrouhlický, D. 2012, *AJ*, 144, 60
- O'Rourke, L., Müller, T., Valtchanov, I., et al. 2012, *Planet. Space Sci.*, 66, 192
- Ostro, S. J., Margot, J.-L., Benner, L. A. M., et al. 2006, *Science*, 314, 1276
- Oszkiewicz, D. A., Muinenen, K., Bowell, E., et al. 2011, *J. Quant. Spec. Radiat. Transf.*, 112, 1919
- Pajuelo, M., Carry, B., Vachier, F., et al. 2018, *Icarus*, 309, 134
- Parker, A., Ivezić, Ž., Jurić, M., et al. 2008, *Icarus*, 198, 138
- Pätzold, M., Andert, T. P., Asmar, S. W., et al. 2011, *Science*, 334, 491
- Pedregosa, F., Varoquaux, G., Gramfort, A., et al. 2011, *Journal of Machine Learning Research*, 12, 2825
- Penttilä, A., Shevchenko, V. G., Wilkman, O., & Muinenen, K. 2016, *Planet. Space Sci.*, 123, 117
- Perna, D., Barucci, M. A., Fulchignoni, M., et al. 2018, *Planet. Space Sci.*, 157, 82
- Popescu, M., Licandro, J., Carvano, J. M., et al. 2018, *A&A*, 617, A12
- Pravec, P., Fatka, P., Vokrouhlický, D., et al. 2019, *Icarus*, 333, 429
- Pravec, P., Vokrouhlický, D., Polishook, D., et al. 2010, *Nature*, 466, 1085
- Pravec, P., Šarounová, L., Rabinowitz, D. L., et al. 2000, *Icarus*, 146, 190
- Rocher, P. & Cavellier, C. 1996, in *Dynamics, Ephemerides, and Astrometry of the Solar System*, ed. S. Ferraz-Mello, B. Morando, & J.-E. Arlot, Vol. 172, 357
- Rodrigo, C. & Solano, E. 2020, in XIV.0 Scientific Meeting (virtual) of the Spanish Astronomical Society, 182
- Rodrigo, C., Solano, E., & Bayo, A. 2012, SVO Filter Profile Service Version 1.0, IVOA Working Draft 15 October 2012
- Rozitis, B. & Green, S. F. 2014, *A&A*, 568, A43
- Rozitis, B., Green, S. F., MacLennan, E., & Emery, J. P. 2018, *MNRAS*, 477, 1782
- Sanchez, J. A., Reddy, V., Nathues, A., et al. 2012, *Icarus*, 220, 36
- Scheeres, D. J. 2007, *Icarus*, 189, 370
- Scheeres, D. J., Britt, D., Carry, B., & Holsapple, K. A. 2015, *Asteroid Interiors and Morphology*, ed. P. Michel, F. DeMeo, & W. F. Bottke (Univ. Arizona Press), 745–766
- Scheirich, P. & Pravec, P. 2009, *Icarus*, 200, 531
- Schubart, J. 1974, *A&A*, 30, 289
- Sergeyev, A. V. & Carry, B. 2021, *A&A*, 652, A59
- Sergeyev, A. V., Carry, B., Onken, C. A., et al. 2022, *A&A*, 658, A109
- Shepard, M. K., Timerson, B., Scheeres, D. J., et al. 2018, *Icarus*, 311, 197
- Shevchenko, V. G., Belskaya, I. N., Muinenen, K., et al. 2016, *Planet. Space Sci.*, 123, 101
- Siltala, L. & Granvik, M. 2020, *A&A*, 633, A46
- Skrutskie, M. F., Cutri, R. M., Stiening, R., et al. 2006, *AJ*, 131, 1163
- Slivan, S. M. 2002, *Nature*, 419, 49
- Snodgrass, C., Carry, B., Dumas, C., & Hainaut, O. 2010, *A&A*, 511, A72
- Solem, J. C. 1994, *Nature*, 370, 349
- Standish, E. M. & Hellings, R. W. 1989, *Icarus*, 80, 326
- Sykes, M. V., Cutri, R. M., Fowler, J. W., et al. 2000, *Icarus*, 146, 161
- Tanga, P., Carry, B., Colas, F., et al. 2015, *MNRAS*, 448, 3382
- Taylor, M. B. 2005, in *Astronomical Society of the Pacific Conference Series*, Vol. 347, *Astronomical Data Analysis Software and Systems XIV*, ed. P. Shopbell, M. Britton, & R. Ebert, 29
- Tedesco, E. F. 1989, in *Asteroids II*, ed. R. P. Binzel, T. Gehrels, & M. S. Matthews, 1090–1138
- Tedesco, E. F., Noah, P. V., Noah, M., & Price, S. D. 2002, *AJ*, 123, 1056
- Tedesco, E. F., Williams, J. G., Matson, D. L., et al. 1989, in *Asteroids II*, ed. R. P. Binzel, T. Gehrels, & M. S. Matthews, 1151–1161
- Tholen, D. J. 1984, PhD thesis, University of Arizona
- Tholen, D. J. 1989, in *Asteroids II*, ed. R. P. Binzel, T. Gehrels, & M. S. Matthews, 1139–1150
- Tisserand, F. 1889, *Bulletin Astronomique, Serie I*, 6, 241
- Tsirvoulis, G. 2019, *MNRAS*, 482, 2612
- Vachier, F., Berthier, J., & Marchis, F. 2012, *A&A*, 543, A68
- Vasavada, A. R., Paige, D. A., & Wood, S. E. 1999, *Icarus*, 141, 179
- Đurech, J., Delbo', M., Carry, B., Hanuš, J., & Alí-Lagoa, V. 2017, *A&A*, 604, A27
- Đurech, J., Kaasalainen, M., Herald, D., et al. 2011, *Icarus*, 214, 652
- Veeder, G. J., Matson, D. L., & Tedesco, E. F. 1983, *Icarus*, 55, 177
- Vernazza, P., Brož, M., Drouard, A., et al. 2018, *A&A*, 618, A154
- Viikinkoski, M., Kaasalainen, M., & Durech, J. 2015, *A&A*, 576, A8
- Vinogradova, T. A. 2019, *MNRAS*, 484, 3755
- Vokrouhlický, D., Bottke, W. F., Chesley, S. R., Scheeres, D. J., & Statler, T. S. 2015, *The Yarkovsky and YORP Effects*, ed. P. Michel, F. DeMeo, & W. F. Bottke, 509–531
- Vokrouhlický, D. & Nesvorný, D. 2008, *AJ*, 136, 280
- Žižka, J., Galád, A., Vokrouhlický, D., et al. 2016, *A&A*, 595, A20
- Warner, B. D., Harris, A. W., & Pravec, P. 2021, NASA Planetary Data System, 10
- Wolters, S. D. & Green, S. F. 2009, *MNRAS*, 400, 204
- Wright, E. L., Eisenhardt, P. R. M., Mainzer, A. K., et al. 2010, *AJ*, 140, 1868
- Xu, S., Binzel, R. P., Burbine, T. H., & Bus, S. J. 1995, *Icarus*, 115, 1
- Yeh, T.-S., Li, B., Chang, C.-K., et al. 2020, *AJ*, 160, 73
- Yeomans, D. K., Barriot, J. P., Dunham, D. W., et al. 1997, *Science*, 278, 2106
- Zappala, V., Cellino, A., Farinella, P., & Knezevic, Z. 1990, *AJ*, 100, 2030
- Zappala, V., di Martino, M., Farinella, P., & Paolicchi, P. 1983, in *Asteroids, Comets, and Meteors*, 73–76
- Zellner, B. & Bowell, E. 1977, in *IAU Colloq. 39: Comets, Asteroids, Meteorites: Interrelations, Evolution and Origins*, ed. A. H. Delsemme, 185–195
- Zellner, B. & Gradie, J. 1976, *AJ*, 81, 262
- Zessewitsch, W. 1932, *Astronomische Nachrichten*, 246, 441
- Zinzi, A., Giardino, M., Giunta, A., et al. 2021, in *LPI Contributions*, Vol. 2549, *5th Planetary Data Workshop & Planetary Science Informatics & Analytics*, 7032

Appendix A: Collections available in SsODNet.dataCloud

Table A.1: Description of the collections included in SsODNet.dataCloud.

Name	Description	N	N_{SSO}	Desc.	Reference
astorb	Lowell orbits of asteroids	1 078 203	1 078 203	A.2	Bowell et al. (1994)
colors	Compilation of colors	4 793 938	428 339	A.3	29 references
cometpro	IMCCE orbits of comets	1 613	1 613	A.4	Rocher & Cavelier (1996)
density	Density estimates	49	29	A.5	26 references
diamalbedo	Diameter & albedo estimates	261 396	149 375	A.6	205 references
families	Dynamical families	493 364	261 832	A.7	9 references
masses	Mass estimates	2 170	422	A.8	165 references
mpcatobs	MPC catalog of observations	341 772 068	1 674 187	A.9	MPC (2021)
mpcorb	MPC orbits of asteroids	1 223 386	1 223 386	A.10	Marsden (1980)
pairs	Asteroid pairs	340	236	A.11	12 references
phase_function	Parameters of phase functions	330 279	227 888	A.12	4 references
proper_elements	Proper elements of asteroids	799 878	799 878	A.13	Novakovic & Radovic (2019)
spin	Spin solutions	47 541	28 951	A.14	2 775 references
taxonomy	Taxonomic classes	274 322	140 713	A.15	208 references
thermal_properties	Thermal inertia estimates	4 510	2 109	A.16	57 references
yarkovsky	Yarkovsky drifts	826	578	A.17	17 references
Total		351 083 883	1 223 984		3007 references

For each collection we list the number of entries (N), number of SSOs (N_{SSO}), the reference to a table describing its fields (Desc.), and the number of included bibliographic references.

Table A.2: Description of the fields in the collection astorb of the dataCloud.

#	Field	Type	Description
1	num	int	SSO IAU number
2	name	varchar	SSO name
3	orbit_computer	varchar	Orbit computer
4	H	double	Absolute magnitude (mag)
5	G	double	Slope parameter (Bowell et al., 1989)
6	B_V	double	B-V color (mag) from Tedesco (1989)
7	IRAS_diameter	double	IRAS diameter (km) from Tedesco et al. (1989)
8	IRAS_class	varchar	IRAS taxonomic classification from Tedesco et al. (1989)
9	note_1	int	Categories of planet-crossing asteroids
10	note_2	int	Assumptions for orbit computation
11	note_3	int	Asteroids observed during the course of major surveys
12	note_4	int	Indication from MPC critical-list of numbered asteroids
13	note_5	int	Discoveries at Lowell Observatory and related discoveries
14	note_6	int	Rank for Lowell collaborative program of astrometry
15	orbital_arc	int	Orbital arc spanned by observations used in orbit computation (days)
16	number_observation	int	Number of observations used in orbit computation
17	yy_osc	int	Year of the epoch of osculation
18	mm_osc	int	Month of the epoch of osculation
19	dd_osc	int	Day of the epoch of osculation
20	mean_anomaly	double	Mean anomaly (deg)
21	perihelion_argument	double	Argument of perihelion (deg) in ECJ2000.0

Table A.2: continued.

#	Field	Type	Description
22	node_longitude	double	Longitude of ascending node (deg) in ECJ2000.0
23	inclination	double	Inclination (deg) in ECJ2000.0
24	eccentricity	double	Eccentricity
25	semi_major_axis	double	Semi-major axis (au)
26	YY_calculation	int	Year of the date of orbit computation
27	MM_calculation	int	Month of the date of orbit computation
28	DD_calculation	int	Day of the date of orbit computation
29	CEU_value	double	Absolute value of the Current 1- σ Ephemeris Uncertainty (CEU, in arcsec)
30	CEU_rate	double	Rate of change of CEU (arcsec/day)
31	CEU_yy	int	Year of the date of CEU
32	CEU_mm	int	Month of the date of CEU
33	CEU_dd	int	Day of the date of CEU
34	PEU_value	double	Next Peak Ephemeris Uncertainty (PEU) from date of CEU (arcsec)
35	PEU_yy	int	Year of the date of occurrence of the PEU
36	PEU_mm	int	Month of the date of occurrence of the PEU
37	PEU_dd	int	Day of the date of occurrence of the PEU
38	GPEU_fromCEU	double	Greatest PEU in 10 years from date of CEU (arcsec)
39	GPEU_yy	int	Year of the date of occurrence of the GPEU
40	GPEU_mm	int	Month of the date of occurrence of the GPEU
41	GPEU_dd	int	Day of the date of occurrence of the GPEU
42	GPEU_fromPEU	double	Greatest PEU in 10 years from date of next PEU (arcsec)
43	GGPEU_yy	int	Year of the date of occurrence of the GPEU from PEU
44	GGPEU_mm	int	Month of the date of occurrence of the GPEU from PEU
45	GGPEU_dd	int	Day of the date of occurrence of the GPEU from PEU
46	jd_osc	double	JD of the epoch of osculation
47	px	double	x component of the EQJ2000 heliocentric position vector (au)
48	py	double	y component of the EQJ2000 heliocentric position vector (au)
49	pz	double	z component of the EQJ2000 heliocentric position vector (au)
50	vx	double	x component of the EQJ2000 heliocentric velocity vector (au/d)
51	vy	double	y component of the EQJ2000 heliocentric velocity vector (au/d)
52	vz	double	z component of the EQJ2000 heliocentric velocity vector (au/d)
53	mean_motion	double	Mean motion (deg/d)
54	orbital_period	double	Orbital period (d)
55	iddataset	int	Bibliographic unique reference

Fields follow the original ASTORB data (Bowell et al., 1994), and we refer to the online documentation for further details on each field (<https://asteroid.lowell.edu/main/astorb/>).

Table A.3: Description of the fields in the collection colors of the dataCloud.

#	Field	Type	Description
1	num	int	SSO IAU number
2	name	varchar	SSO name
3	color	varchar	Name of the color (e.g, B-V)
4	value	double	Value of the color
5	uncertainty	double	Uncertainty on the color
6	facility	varchar	Source of data (telescope, survey)
7	observer	varchar	Observer IAU code
8	epoch	double	Epoch of observation (JD)
9	delta_time	float	Time difference between filters (s)
10	color_type	varchar	Description of the method (Table B.1)

Table A.3: continued.

#	Field	Type	Description
11	id_filter_1	varchar	First filter unique identifier (SVO filter service, Rodrigo et al., 2012)
12	id_filter_2	varchar	Second filter unique identifier (SVO filter service, Rodrigo et al., 2012)
13	phot_sys	varchar	Photometric system (Vega, AB, ST)
14	selection	int	Selection flag (Section 4)
15	iddataset	int	Bibliographic unique reference

Table A.4: Description of the fields in the collection cometpro of the dataCloud.

#	Field	Type	Description
2	note	int	Number of the note associated with the comet
3	updated	date	Date of update (DD/MM/YYYY)
4	name	varchar	IAU code of the comet
5	iau_name	varchar	IAU name of the comet
6	author	varchar	Orbit computer
7	epoch	double	Reference epoch of the orbit (JD)
8	force_relat	int	Relativity effect of the Sun taken into account (1) or not (0)
9	nb_obs	int	Number of observations used in orbit computation
10	sigma	double	1-sigma residual (arcsec)
11	start_date	date	Date of first observation used in orbit computation (DD/MM/YYYY)
12	end_date	date	Date of last observation used in orbit computation (DD/MM/YYYY)
13	px	double	x component of the EQJ2000 heliocentric position vector (au)
14	py	double	y component of the EQJ2000 heliocentric position vector (au)
15	pz	double	z component of the EQJ2000 heliocentric position vector (au)
16	vx	double	x component of the EQJ2000 heliocentric velocity vector (au/d)
17	vy	double	y component of the EQJ2000 heliocentric velocity vector (au/d)
18	vz	double	z component of the EQJ2000 heliocentric velocity vector (au/d)
19	fng_A1	double	Radial non-gravitational acceleration (heliocentric EQJ2000)
20	fng_A2	double	Tangential non-gravitational acceleration (heliocentric EQJ2000)
21	fng_A3	double	Normal non-gravitational acceleration (heliocentric EQJ2000)
22	tau	double	Date of perihelion passage (JD)
23	perihelion_distance	double	Perihelion distance (au)
24	eccentricity	double	Eccentricity
25	perihelion_argument	double	Argument of perihelion (deg) (J2000.0)
26	node_longitude	double	Longitude of the ascending node (deg) (J2000.0)
27	inclination	double	Inclination to ecliptic (deg) (J2000.0)
28	mag_H1	double	Constant term of magnitude to compute the total magnitude
29	mag_R1	double	Coefficient of log(r) to compute the total magnitude
30	mag_D1	double	Coefficient of log(Delta) to compute the total magnitude
31	mag_H2	double	Constant term of magnitude to compute the nuclear magnitude
32	mag_R2	double	Coefficient of log(r) to compute the nuclear magnitude
33	mag_D2	double	Coefficient of log(Delta) to compute the nuclear magnitude
34	selection	int	Selection flag (Section 4)
35	iddataset	int	Bibliographic unique reference

Fields follow the original COMETPRO data ([Rocher & Cavelier, 1996](#)).

Table A.5: Description of the fields in the collection `density` of the `dataCloud`.

#	Field	Type	Description
1	<code>num</code>	<code>int</code>	SSO IAU number
2	<code>name</code>	<code>varchar</code>	SSO name
3	<code>density</code>	<code>double</code>	Density in $\text{kg}\cdot\text{m}^{-3}$
4	<code>err_density_up</code>	<code>double</code>	Upper uncertainty on the density ($\text{kg}\cdot\text{m}^{-3}$)
5	<code>err_density_down</code>	<code>double</code>	Lower uncertainty on the density ($\text{kg}\cdot\text{m}^{-3}$)
6	<code>method</code>	<code>varchar</code>	Description of the method (Table B.1)
7	<code>selection</code>	<code>int</code>	Selection flag (Section 4)
8	<code>iddataset</code>	<code>int</code>	Bibliographic unique reference

Table A.6: Description of the fields in the collection `diameterbedo` of the `dataCloud`.

#	Field	Type	Description
1	<code>num</code>	<code>int</code>	SSO IAU number
2	<code>name</code>	<code>varchar</code>	SSO name
3	<code>diameter</code>	<code>double</code>	Diameter in km
4	<code>err_diameter_up</code>	<code>double</code>	Upper uncertainty on the diameter (km)
5	<code>err_diameter_down</code>	<code>double</code>	Lower uncertainty on the diameter (km)
6	<code>albedo</code>	<code>double</code>	Geometric visual albedo
7	<code>err_albedo_up</code>	<code>double</code>	Upper uncertainty on the albedo
8	<code>err_albedo_down</code>	<code>double</code>	Lower uncertainty on the albedo
9	<code>beaming</code>	<code>double</code>	Beaming parameter (Harris & Davies, 1999)
10	<code>err_beaming</code>	<code>double</code>	Uncertainty on the beaming parameter
11	<code>emissivity</code>	<code>double</code>	Emissivity (Harris & Davies, 1999)
12	<code>err_emissivity</code>	<code>double</code>	Uncertainty on the emissivity
13	<code>selection</code>	<code>int</code>	Selection flag (Section 4)
14	<code>method</code>	<code>varchar</code>	Description of the method (Table B.1)
15	<code>iddataset</code>	<code>int</code>	Bibliographic unique reference

Table A.7: Description of the fields in the collection `family` of the `dataCloud`.

#	Field	Type	Description
1	<code>num</code>	<code>int</code>	SSO IAU number
2	<code>name</code>	<code>varchar</code>	SSO name
3	<code>family_status</code>	<code>varchar</code>	SSO status: core, halo, diffuse halo
4	<code>family_num</code>	<code>int</code>	IAU number of the family (if named after an asteroid)
5	<code>family_name</code>	<code>varchar</code>	Name of the family
6	<code>selection</code>	<code>int</code>	Selection flag (Section 4)
7	<code>method</code>	<code>varchar</code>	Description of the method (Table B.1)
8	<code>iddataset</code>	<code>int</code>	Bibliographic unique reference

Table A.8: Description of the fields in the collection `masses` of the `dataCloud`.

#	Field	Type	Description
1	<code>num</code>	<code>int</code>	SSO IAU number
2	<code>name</code>	<code>varchar</code>	SSO name
3	<code>mass</code>	<code>double</code>	Mass in kg
4	<code>err_mass_up</code>	<code>double</code>	Upper uncertainty on the mass (kg)
5	<code>err_mass_down</code>	<code>double</code>	Lower uncertainty on the mass (kg)

Table A.8: continued.

#	Field	Type	Description
6	method	varchar	Description of the method (Table B.1)
7	selection	int	Selection flag (Section 4)
8	method	varchar	Description of the method (Table B.1)
9	iddataset	int	Bibliographic unique reference

Table A.9: Description of the fields in the collection mpcatobs of the dataCloud.

#	Field	Type	Description
1	type	varchar	Type of SSO (asteroid, comet)
2	num	varchar	SSO number
3	packed_name	varchar	SSO packed name
4	name	varchar	SSO name
5	orbit_type	varchar	Type of orbit (for comets)
6	discovery	varchar	Discovery asterisk
7	note1	varchar	See MPC Web site
8	note2	varchar	See MPC Web site
9	date_obs	datetime	Date of observation (ISO)
10	jd_obs	double	Date of observation (JD)
11	ra_obs	double	Observed right ascension (deg) (EQJ2000.0)
12	dec_obs	double	Observed declination (deg) (EQJ2000.0)
13	mag	double	Observed magnitude (mag)
14	filter	varchar	Magnitude band
15	astrocata_name	varchar	Astrometric reference catalog used to determine the position
16	astrocata_vizname	varchar	VizieR table base-name of the astrometric reference catalog
17	mpc_ref	varchar	Permanent references to the MPCs, MPSs, or other journals
18	iau_code	varchar	IAU observatory code
19	obs_long	double	Geographic longitude of observing site (deg)
20	obs_lat	double	Geographic latitude of observing site (deg)
21	obs_alt	double	Altitude of observing site (m)
22	vgs_x	double	x component of spacecraft geocentric position vector (au) (EQJ2000.0)
23	vgs_y	double	y component of spacecraft geocentric position vector (au) (EQJ2000.0)
24	vgs_z	double	z component of spacecraft geocentric position vector (au) (EQJ2000.0)
25	iddataset	int	Bibliographic unique reference

MPC Web site: <https://minorplanetcenter.net/iau/info/OpticalObs.html>

Table A.10: Description of the fields in the collection mpcorb of the dataCloud.

#	Field	Type	Description
1	packed_name	varchar	Packed number or name of the SSO
2	num	int	SSO IAU Number
3	name	varchar	SSO name
4	H	double	Absolute magnitude (mag)
5	G	double	Slope parameter (Bowell et al., 1989)
6	ref_date	datetime	Reference epoch TT (ISO)
7	mean_anomaly	double	Mean anomaly (deg)
8	perihelion_argument	double	Argument of perihelion (deg) in ECJ2000.0
9	node_longitude	double	Longitude of ascending node (deg) ECJ2000.0
10	inclination	double	Inclination (deg) in ECJ2000.0
11	eccentricity	double	Eccentricity

Table A.10: continued.

#	Field	Type	Description
12	mean_motion	double	Mean motion (deg/d)
13	semi_major_axis	double	Semi-major axis (au)
14	U	varchar	Uncertainty parameter
15	reference	varchar	Orbit reference
16	number_observation	int	Number of observations used to compute the orbit
17	number_opposition	int	Number of oppositions
18	start_obs	int	Year of the first observation
19	end_obs	int	Year of the last observation
20	orbital_arc	double	Orbit arc length (d)
21	rms	double	Root-mean square residuals of the fit (arcsec)
22	coarse_indic	varchar	Coarse indicator of perturbers
23	precise_indic	varchar	Precise indicator of perturbers
24	orbit_computer	varchar	Orbit computer
25	orbit_type	varchar	4-hexdigit flags describing the orbit
26	last_obs	double	Date of last observation included in orbit solution (YYYYMMDD)
27	jd_osc	double	JD of the epoch of osculation
28	px	double	x component of heliocentric position vector (au, EQJ2000)
29	py	double	y component of heliocentric position vector (au, EQJ2000)
30	pz	double	z component of heliocentric position vector (au, EQJ2000)
31	vx	double	x component of heliocentric velocity vector (au/d, EQJ2000)
32	vy	double	y component of heliocentric velocity vector (au/d, EQJ2000)
33	vz	double	z component of heliocentric velocity vector (au/d, EQJ2000)
34	orbital_period	double	Orbital period (d)
35	iddataset	int	Bibliographic unique reference

Fields follows the original MPCORB data, see the online documentation <https://www.minorplanetcenter.net/iau/info/MPOrbitFormat.html>.

Table A.11: Description of the fields in the collection pairs of the dataCloud.

#	Field	Type	Description
1	num	int	First member IAU number
2	name	varchar	First member name
3	sibling_num	int	Second member IAU number
2	sibling_name	varchar	Second member name
3	distance	double	Orbital distance (m/s)
4	age	double	Estimated age of the pair (kyr)
4	err_age_up	double	Upper uncertainty on the age (kyr)
5	err_age_down	double	Lower uncertainty on the age (kyr)
7	selection	int	Selection flag (Section 4)
6	method	varchar	Description of the method (Table B.1)
8	iddataset	int	Bibliographic unique reference

Table A.12: Description of the fields in the collection phase_function of the dataCloud.

#	Field	Type	Description
1	num	int	SSO IAU Number
2	name	varchar	SSO name
3	H	double	Absolute magnitude
4	G1	double	Phase parameter G_1 (Muinonen et al., 2010)

Table A.12: continued.

#	Field	Type	Description
5	G2	double	Phase parameter G ₂ (Muinonen et al., 2010)
6	err_H_down	double	Lower uncertainty on absolute magnitude
7	err_H_up	double	Upper uncertainty on absolute magnitude
8	err_G1_down	double	Lower uncertainty on G ₁ phase parameter
9	err_G1_up	double	Upper uncertainty on G ₁ phase parameter
10	err_G2_down	double	Lower uncertainty on G ₂ phase parameter
11	err_G2_up	double	Upper uncertainty on G ₂ phase parameter
12	N	double	Number of observations used to derive (H,G ₁ ,G ₂)
13	phase_min	double	Minimum phase angle (°)
14	phase_max	double	Maximum phase angle (°)
15	rms	double	Root mean-square of the fit (mag)
16	facility	vchar	Source of observations (telescope, survey)
17	name_filter	vchar	Name of the filter
18	id_filter	vchar	Filter unique identifier (SVO filter service, Rodrigo et al., 2012)
19	method	vchar	Description of the method (Table B.1)
20	selection	int	Selection flag (Section 4)
21	iddataset	int	Bibliographic unique reference

Table A.13: Description of the fields in the collection `proper_elements` of the `dataCloud`.

#	Field	Type	Description
1	num	int	SSO IAU Number
2	name	vchar	SSO name
3	H	double	Absolute magnitude
4	proper_semi_major_axis	double	Proper semi-major axis (au)
5	err_proper_semi_major_axis	double	Uncertainty on proper semi-major axis (au)
6	proper_eccentricity	double	Proper eccentricity
7	err_proper_eccentricity	double	Uncertainty on proper eccentricity
8	proper_sine_inclination	double	Sine of proper inclination
9	err_proper_sine_inclination	double	Uncertainty on sine of proper inclination
10	proper_inclination	double	Proper inclination (°)
11	err_proper_inclination	double	Uncertainty on proper inclination (°)
12	proper_frequency_mean_motion	double	Proper frequency of mean motion (°/yr)
13	err_proper_frequency_mean_motion	double	Uncertainty on proper frequency of mean motion (°/yr)
14	proper_frequency_perihelion_longitude	double	Proper frequency of perihelion longitude (arcsec/yr)
15	err_proper_frequency_perihelion_longitude	double	Uncertainty on proper frequency of perihelion longitude (arcsec/yr)
16	proper_frequency_nodal_longitude	double	Proper frequency of nodal longitude (arcsec/yr)
17	err_proper_frequency_nodal_longitude	double	Uncertainty on proper frequency of nodal longitude (arcsec/yr)
18	lyapunov_time	double	Timescale of chaoticity (yr)
19	integration_time	double	Length of integration (Myr)
20	identfrom	vchar	Name of the SSO in the imported data
21	iddataset	int	Bibliographic unique reference

Table A.14: Description of the fields in the collection `spin` of the `dataCloud`.

#	Field	Type	Description
1	num	int	SSO IAU number
2	name	vchar	SSO name
3	model_name	vchar	Name of the model
4	t0	double	Reference epoch for spin coordinates (JD)
5	W0	double	Rotation phase at t0 ($^{\circ}$, Archinal et al., 2018)
6	Wp	double	Rotation velocity ($^{\circ}/d$, Archinal et al., 2018)
7	RA0	double	EQJ2000 right ascension of the spin axis ($^{\circ}$)
8	DEC0	double	EQJ2000 declination of the spin axis ($^{\circ}$)
9	err_RA0	double	Uncertainty on the right ascension ($^{\circ}$)
10	err_DEC0	double	Uncertainty on the declination ($^{\circ}$)
11	period	double	Rotation period (h)
12	err_period	double	Uncertainty on rotation period (h)
13	period_flag	double	Rotation period quality code (Warner et al., 2021)
14	period_type	vchar	Sidereal or synodic
15	long	double	ECJ2000 longitude of the spin axis ($^{\circ}$)
16	lat	double	ECJ2000 latitude of the spin axis ($^{\circ}$)
17	err_long	double	Uncertainty on the longitude ($^{\circ}$)
18	err_lat	double	Uncertainty on the latitude ($^{\circ}$)
19	selection	int	Selection flag (Section 4)
20	method	vchar	Description of the method (Table B.1)
21	iddataset	int	Bibliographic unique reference

Table A.15: Description of the fields in the collection `taxonomy` of the `dataCloud`.

#	Field	Type	Description
1	num	int	SSO IAU number
2	name	vchar	SSO name
3	scheme	vchar	Taxonomic scheme (e.g., Tholen, Bus, DeMeo, Mahlke)
4	class	vchar	Taxonomic class
5	complex	vchar	Taxonomic complex (Table C.8)
6	selection	int	Selection flag (Section 4)
7	method	vchar	Description of the method (Table B.1)
8	wavrange	vchar	Wavrange used in taxonomy (VIS, NIR, VISNIR)
9	iddataset	int	Bibliographic unique reference

Table A.16: Description of the fields in the collection `thermal_properties` of the `dataCloud`.

#	Field	Type	Description
1	num	int	SSO IAU number
2	name	vchar	SSO name
3	TI	double	Thermal inertia ($J.s^{-1/2}K^{-1}m^{-2}$)
4	err_TI_up	double	Upper uncertainty on the thermal inertia
5	err_TI_down	double	Lower uncertainty on the thermal inertia
6	dsun	double	Heliocentric distance at the time of measurements (au)
7	selection	int	Selection flag (Section 4)
8	method	vchar	Description of the method (Table B.1)
9	iddataset	int	Bibliographic unique reference

Table A.17: Description of the fields in the collection yarkovsky of the dataCloud.

#	Field	Type	Description
1	num	int	SSO IAU Number
2	name	vvarchar	SSO name
3	A2	double	Radial acceleration (10^{-15} au/ d^2)
4	err_A2	double	Uncertainty on radial acceleration (10^{-15} au/ d^2)
5	dadt	double	Semi-major drift (10^{-4} au/Myr)
6	err_dadt	vvarchar	Uncertainty on semi-major drift (10^{-4} au/Myr)
7	snr	float	Signal-to-noise ratio
8	S	float	Sensitivity parameter (Nugent et al., 2012)
9	selection	int	Selection flag (Section 4)
10	method	vvarchar	Description of the method (Table B.1)
11	iddataset	int	Bibliographic unique reference

Appendix B: Description of all the methods

Table B.1: Methods included in SsODNet.

Method	Name	Description	Reference
SPACE	Rendez-vous with a spacecraft	The results are based on data which had an encounter (flyby or orbit) with the target	Belton et al. (1992)
STM	Standard Thermal Model	Diameter and albedo derived by fitting mid-infrared data with a simple thermal model of non-rotating spheres	Lebofsky et al. (1986)
NEATM	Near-Earth Asteroid Thermal Model	Diameter, albedo, beaming derived by fitting mid-infrared data with a simple thermal model	Harris & Davies (1999)
TPM	ThermoPhysical Model	Diameter, albedo, thermal inertia derived by fitting mid-infrared data with a thermal model taking into account the spin, shape of the target	Lagerros (1996)
PhaseFunction	Albedo determined from the phase function	Albedo determined from the phase function	Belskaya & Shevchenko (2000)
LC	Lightcurve	Rotation period determined from optical light curves	Zesewitsch (1932)
Comet-Break	Mass from break-up	Mass estimated from the break-up of the comet	Solem (1994)
FRM	Fast Rotating Model	Diameter and albedo derived by fitting mid-infrared data with a simple thermal model of rapidly non-rotating spheres	Lebofsky & Spencer (1989)
NESTM	Night Emission Simulated Thermal Model	Diameter, albedo, beaming derived by fitting mid-infrared data with an adapted NEATM	Wolters & Green (2009)
Speckle	Triaxial ellipsoid from speckle interferometry	3D shape modeled as tri-axial ellipsoid using speckle interferometry	Drummond et al. (1985)
Interferometry	Optical and Infrared Interferometry	Diameter derived from interferometric visibilities in the optical or infrared	Delbo et al. (2009)
Occ	Stellar Occultation	Apparent size measured during a stellar occultation	Dunham & Mallen (1979)
IM	Apparent shape from direct imaging	Apparent size/shape measured on disk-resolved images	Marchis et al. (2006)
IM-PSF	Diameter from PSF deviation	Estimate of diameter from the deviation of the PSF compared with a star	Brown & Trujillo (2004)
TE-IM	Triaxial ellipsoid from disk-resolved imaging	3D shape modeled as tri-axial ellipsoid using disk-resolved images	Drummond (2000)
TE-Occ	Triaxial ellipsoid from stellar occultation	3D shape modeled as tri-axial ellipsoid using stellar occultations	Drummond & Cocke (1989)
ADAM	All-Data Asteroid Model	3D shape model obtained from a combined use of stellar occultations, optical light curves, disk-resolved images, interferometric fringes	Viikinkoski et al. (2015)
KOALA	Knitted Occultation, Adaptive-optics, and Lightcurves Analysis	The results are obtained from the combined use of stellar occultation, optical light curves, and disk-resolved images	Carry et al. (2010)

Table B.1: continued.

Method	Name	Description	Reference
Radar	Radar shape modeling	3D shape model based on radar Delay-Doppler data	Hudson & Ostro (1994)
Radar-LC	Combined radar and light curve shape modeling	3D shape model based on radar Delay-Doppler and optical light curve data	Hudson et al. (1997)
SAGE	Shaping Asteroids with Genetic Evolution	3D shape model based on light curves, found by genetic evolution	Bartczak & Dudziński (2018)
Polarimetry	Albedo determined from polarimetry	Albedo determined from polarimetry	Cellino et al. (1999)
A-M	Amplitude-Magnitude	Determination of the spin axis from the amplitude of light curves	Zappala et al. (1983)
TE	Triaxial ellipsoid from light curves	Determination of the spin axis, modeling the light curves with a triaxial ellipsoid	Hanuš et al. (2021)
LCI	Lightcurve Inversion	Spin and convex 3-D shape determined from optical light curves	Kaasalainen & Torppa (2001)
LC+Occ	Scaling of Lightcurve Inversion Model with Stellar Occultations	3D shape model from light-curve inversion scaled using stellar occultation(s)	Ďurech et al. (2011)
LC+IM	Scaling of Lightcurve Inversion Model with direct imaging	3D shape model from a light-curve inversion scaled using disk-resolved image(s)	Hanuš et al. (2013b)
LC+TPM	Scaling of light-curve inversion model with the thermophysical model	3D shape model from a light-curve inversion scaled using a thermophysical model on mid-infrared data	Hanuš et al. (2015)
LC-TPM	Combined light-curve inversion and thermophysical modeling	3D shape modeling from simultaneous a light-curve inversion and thermophysical model of mid-infrared data	Ďurech et al. (2017)
EPHEM	Mass from ephemerides	The mass is determined from general ephemerides of the Solar System	Baer & Chesley (2008)
DEFLECT	Mass from close encounter deflection	The mass is determined from the orbital deflection of smaller asteroids	Standish & Hellings (1989)
Bin-IM	Mass from optical imaging a binary system	Mass from a binary system imaged in the optical	Merline et al. (1999)
Bin-Radar	Mass from radar observations of a binary system	Mass from a binary system observed by radar echoes	Ostro et al. (2006)
Bin-PheMu	Mass from mutual phenomena in a binary system	Mass from a binary system from the timings and shape of mutual event from light curves	Pravec et al. (2000)
Bin-Genoid	Orbit and mass from a multiple asteroidal system using Genoid algorithm	Orbital elements and mass determination from a multiple asteroidal system with Genoid	Vachier et al. (2012)
Yarkovsky	Mass from Yarkovsky drift	Determination of the mass from the measured Yarkovsky drift	Chesley et al. (2014)
Comet-NGF	Mass from non-gravitational forces	Mass estimated from the non-gravitational acceleration	Davidsson et al. (2007)
Spec	Reflectance spectroscopy	Reflectance spectroscopy	McCord et al. (1970)
Phot	Multi-filter photometry	Multi-band photometry	DeMeo & Carry (2013)

Table B.1: continued.

Method	Name	Description	Reference
Astrometry(0)	Yarkovsky drift from optical astrometry	Determination of the semi-major drift due to Yarkovsky using astrometry from optical observations	Chesley et al. (2003)
Astrometry(0+R)	Yarkovsky drift from optical astrometry and radar delays	Determination of the semi-major drift due to Yarkovsky using astrometry from optical observations and radar delays	Chesley et al. (2003)
Family_age	Yarkovsky drift from family age	Determination of the semi-major drift due to Yarkovsky using the age of the dynamical family	Carruba et al. (2017)
HCM	Hierarchical Clustering Method	Determination of family membership by hierarchical clustering of proper elements	Zappala et al. (1990)
V-Shape	Yarkovsky V-shape identification of asteroid families	Determination of family membership by identification of the Yarkovsky print in (semi-major axis, 1/diameter) plane	Bolin et al. (2017)
abs	Colors derived from absolute magnitudes	Colors computed from the absolute magnitudes in the two filters	Mahlke et al. (2021)
lc_cor	Colors derived from apparent magnitudes corrected for light curves	Colors computed from the apparent magnitudes, corrected for short-term variability introduced by light curves	Erasmus et al. (2019)
app	Colors derived from apparent magnitudes	Colors computed from the apparent magnitudes	Sykes et al. (2000)
Yarkovsky_drift	Thermal inertia derived from Yarkovsky drift	Determination of the thermal inertia based on the measured strength of the Yarkovsky effect	Fenucci et al. (2021)
serendipitous	Phase curve from serendipitous observations	Determination of the parameters of the phase function from serendipitous observations (from surveys)	Oszkiewicz et al. (2011)
targeted	Phase curve from targeted observations	Determination of the parameters of the phase function from targeted observations (generally a reduction to the light curve maxima)	Gehrels (1956)

Appendix C: Method lists for best-estimate determination

Table C.1: Ranking of methods for diameter estimates (diamalbedo).

Order	Methods
1	SPACE
2	ADAM, KOALA, SAGE, Radar
3	LC+Occ, LC+IM, LC+TPM, TPM, TE-IM, TE-Occ
4	IM, Occ, IM-PSF, Interferometry
5	NEATM, NESTM
6	STM, FRM
7	Polarimetry

The order favors direct measurements first, then estimates based on 3D shape models, followed by direct measurements limited to a single geometry, and, finally, indirect estimates from thermal model of spheres.

Table C.2: Selection order for albedo determinations (diamalbedo).

Order	Methods
1	SPACE
2	Polarimetry

Table C.3: Selection order for mass determinations (masses).

Order	Methods
1	SPACE
2	Bin-Genoid
3	Bin-IM, Bin-Radar, Bin-PheMu
4	Deflect, Ephem
5	Yarkovsky

The order favors spacecraft encounters, followed by binary systems, and, finally, estimates based on long-distance gravitational interactions and Yarkovsky drift.

Table C.4: Ranking of methods for spin properties (spin).

Order	Methods
1	SPACE
2	ADAM, KOALA, SAGE, Radar, Radar-LC
3	LC+TPM, LC-TPM, LC+IM, LC+Occ
4	LCI
5	LC, A-M, Bin-IM, TE, TE-IM, TE-Occ, Speckle

The order favors solutions from spacecrafts encounters, followed by 3D shape modeling, ranked from modeling including direct measurement to scaling of 3D convex models, to convex model of arbitrary size. Simple ellipsoids follow and, finally, the periods from light curves.

Table C.5: Selection order for colors (colors).

Order	Methods
1	Absolute
2	Light-curve corrected
3	Apparent

The order favors absolute magnitude over light-curve corrected magnitude, and, finally, over apparent magnitude.

Table C.6: Ranking of methods for thermal properties (`thermal_properties`).

Order	Methods
1	SPACE
2	LCI-TPM, LCI+TPM
3	TPM
4	Yarkovsky_drift

The order favors estimates from space mission encounters, then thermophysical models based on 3D shapes, and, finally, estimates from thermophysical models based on limited shape and spin information.

Table C.7: Selection order for Yarkovsky drift determinations (`yarkovsky`).

Order	Methods
1	Astrometry(O+R)
2	Astrometry(O)
3	Family_age

The order favors solutions using a combination of optical and radar observations over optical-only data sets, and, finally, estimates based on family ages.

Table C.8: Class-complex connections for taxonomy.

Complex	Reference	Classes
A	Veeder et al. (1983)	A
B	Tholen (1984)	B
C	Chapman et al. (1975)	C, Cb, CF, CFB, Cg, CG, Cgx, F, FC, G, GC
Ch	Bus & Binzel (2002)	Caa, Cgh, Ch
D	Gradie & Tedesco (1982)	D
E	Zellner & Gradie (1976)	E
K	Tedesco et al. (1989)	K
L	Bell et al. (1988)	L, Ld
M	Zellner & Gradie (1976)	M
O	Binzel et al. (1993)	O
P	Gradie & Tedesco (1982)	DP, P, PD
Q	Tholen (1984)	Q, QO, Qw
R	Bowell et al. (1978)	R
S	Chapman et al. (1975)	S, SA, Sa, Sk, Sl, SO, Sq, SQ, Sqw, Sr, SR, Srw, SV, Sv, Svw, Sw
T	Zellner & Bowell (1977)	T
V	McCord et al. (1970)	J, V, Vw
X	Tholen (1984)	EM, X, Xc, Xe, Xk, Xn, Xt
Z	Mueller et al. (1992)	Z
U		Ad, AQ, AS, AU, AV, BC, BCF, BCU, BFC, BFU, BFX, Bk, BU, CB, CBU, CD, CDX, CFU, CFXU, CGSU, CGTP, CGU, CL, CO, CP, CPF, CPU, CQ, CS, CSGU, CSU, CTGU, CU, CX, CXF, DCX, DL, Ds, DS, DSU, DT, DTU, DU, DX, DXCU, EU, FBCU, FCB, FCU, FCX, FP, FU, FX, FXU, GS, GU, I, Kl, LA, LQ, LS, MU, OV, PC, PCD, PDC, PF, PU, QRS, QSV, QU, QV, SC, SCTU, SD, SDU, SG, SMU, ST, STD, STGD, STU, SU, SX, TCG, TD, TDG, TDS, TS, TSD, TX, XB, XC, XCU, XD, XDC, XF, XFC, XFCU, XFU, XL, XS, XSC, XSCU, XT, XU

The references indicate where the class or complex archetype was labeled as such for the first time.